NASA/TM—2015-218476

Analyses of Hubble Space Telescope Aluminized-Teflon Multilayer Insulation Blankets Retrieved After 19 Years of Space Exposure

Kim K. de Groh
Glenn Research Center, Cleveland, Ohio

Bruce A. Perry
Ohio Aerospace Institute, Brook Park, Ohio

Jelila S. Mohammed
Goddard Space Flight Center, Greenbelt, Maryland

Bruce A. Banks
Science Application International Corporation, Cleveland, Ohio

February 2015

NASA STI Program . . . in Profile

Since its founding, NASA has been dedicated to the advancement of aeronautics and space science. The NASA Scientific and Technical Information (STI) Program plays a key part in helping NASA maintain this important role.

The NASA STI Program operates under the auspices of the Agency Chief Information Officer. It collects, organizes, provides for archiving, and disseminates NASA's STI. The NASA STI Program provides access to the NASA Technical Report Server—Registered (NTRS Reg) and NASA Technical Report Server—Public (NTRS) thus providing one of the largest collections of aeronautical and space science STI in the world. Results are published in both non-NASA channels and by NASA in the NASA STI Report Series, which includes the following report types:

- TECHNICAL PUBLICATION. Reports of completed research or a major significant phase of research that present the results of NASA programs and include extensive data or theoretical analysis. Includes compilations of significant scientific and technical data and information deemed to be of continuing reference value. NASA counter-part of peer-reviewed formal professional papers, but has less stringent limitations on manuscript length and extent of graphic presentations.

- TECHNICAL MEMORANDUM. Scientific and technical findings that are preliminary or of specialized interest, e.g., "quick-release" reports, working papers, and bibliographies that contain minimal annotation. Does not contain extensive analysis.

- CONTRACTOR REPORT. Scientific and technical findings by NASA-sponsored contractors and grantees.

- CONFERENCE PUBLICATION. Collected papers from scientific and technical conferences, symposia, seminars, or other meetings sponsored or co-sponsored by NASA.

- SPECIAL PUBLICATION. Scientific, technical, or historical information from NASA programs, projects, and missions, often concerned with subjects having substantial public interest.

- TECHNICAL TRANSLATION. English-language translations of foreign scientific and technical material pertinent to NASA's mission.

For more information about the NASA STI program, see the following:

- Access the NASA STI program home page at http://www.sti.nasa.gov

- E-mail your question to help@sti.nasa.gov

- Fax your question to the NASA STI Information Desk at 757-864-6500

- Telephone the NASA STI Information Desk at 757-864-9658

- Write to:
  NASA STI Program
  Mail Stop 148
  NASA Langley Research Center
  Hampton, VA 23681-2199

NASA/TM—2015-218476

Analyses of Hubble Space Telescope Aluminized-Teflon Multilayer Insulation Blankets Retrieved After 19 Years of Space Exposure

Kim K. de Groh
Glenn Research Center, Cleveland, Ohio

Bruce A. Perry
Ohio Aerospace Institute, Brook Park, Ohio

Jelila S. Mohammed
Goddard Space Flight Center, Greenbelt, Maryland

Bruce A. Banks
Science Application International Corporation, Cleveland, Ohio

National Aeronautics and
Space Administration

Glenn Research Center
Cleveland, Ohio 44135

February 2015

Acknowledgments

The authors would like to thank Ben Reed and the HST Project Office at NASA GSFC for their support of this project. We greatly appreciate the opportunity to analyze this unique material and provide the results to the space community. We would also like to thank the following people from GSFC for their contributors to testing and analysis: Bryan Abbamonte, Josh Abel, David Hughes, Kristin McKittrick, Aparna Boddapati, Debbie Thomas and Mollie Powell.

Level of Review: This material has been technically reviewed by technical management.

Available from

NASA STI Program
Mail Stop 148
NASA Langley Research Center
Hampton, VA 23681-2199

National Technical Information Service
5285 Port Royal Road
Springfield, VA 22161
703-605-6000

This report is available in electronic form at http://www.sti.nasa.gov/ and http://ntrs.nasa.gov/

Analyses of Hubble Space Telescope Aluminized-Teflon Multilayer Insulation Blankets Retrieved After 19 Years of Space Exposure

Kim K. de Groh
National Aeronautics and Space Administration
Glenn Research Center
Cleveland, Ohio 44135

Bruce A. Perry
Ohio Aerospace Institute
Brook Park, Ohio 44142

Jelila S. Mohammed
National Aeronautics and Space Administration
Goddard Space Flight Center
Greenbelt, Maryland 20771

Bruce A. Banks
Science Application International Corporation
Cleveland, Ohio 44135

Abstract

Since its launch in April 1990, the Hubble Space Telescope (HST) has made many important observations from its vantage point in low Earth orbit (LEO). However, as seen during five servicing missions, the outer layer of multilayer insulation (MLI) has become increasingly embrittled and has cracked in many areas. In May 2009, during the 5th servicing mission (called SM4), two MLI blankets were replaced with new insulation and the space-exposed MLI blankets were retrieved for degradation analyses by teams at NASA Glenn Research Center (GRC) and NASA Goddard Space Flight Center (GSFC). The retrieved MLI blankets were from Equipment Bay 8, which received direct sunlight, and Equipment Bay 5, which received grazing sunlight. Each blanket was divided into several regions based on environmental exposure and/or physical appearance. The aluminized-Teflon (DuPont, Wilmington, DE) fluorinated ethylene propylene (Al-FEP) outer layers of the retrieved MLI blankets have been analyzed for changes in optical, physical, and mechanical properties, along with chemical and morphological changes. Pristine and as-retrieved samples (materials) were heat treated to help understand degradation mechanisms. When compared to pristine material, the analyses have shown how the Al-FEP was severely affected by the space environment. Most notably, the Al-FEP was highly embrittled, fracturing like glass at strains of 1 to 8 percent. Across all measured properties, more significant degradation was observed for Bay 8 material as compared to Bay 5 material. This paper reviews the tensile and bend-test properties, density, thickness, solar absorptance, thermal emittance, x-ray photoelectron spectroscopy (XPS) and energy dispersive spectroscopy (EDS) elemental composition measurements, surface and crack morphologies, and atomic oxygen erosion yields of the Al-FEP outer layer of the retrieved HST blankets after 19 years of space exposure.

1.0 Introduction

The HST was launched into LEO during STS-31 on April 25, 1990 as the first mission of NASA's Great Observatories program. It is capable of performing observations in the near-ultraviolet, visible, and near-infrared wavelengths and was designed to be serviced on-orbit to upgrade scientific capabilities. Five servicing missions (SM) have taken place, with the last mission occurring in May 2009 after 19 years in space.

Multilayer insulation (MLI) blankets covering over 80 percent of the surface of the HST are important for passive temperature control on-orbit. Aluminized-Teflon (DuPont, Wilmington, DE) fluorinated ethylene propylene (Al-FEP) is used as the outer layer of the MLI thermal control insulation because the FEP outer layer has excellent optical properties (low solar absorptance (α_s) and high thermal emittance (ε)) and the vapor deposited aluminum backing reflects incident solar radiation.

In general, polymers such as Teflon FEP experience degradation in mechanical, electrical, and thermal properties due to exposure to radiation (Ref. 1). Hubble Space Telescope surfaces are exposed to various types of radiation including solar ultraviolet (UV) radiation, x-rays from the Sun, and electron and proton particle radiation. Additionally, the temperature cycling experienced by HST insulation has been found to have an effect on mechanical properties of FEP, especially when passing through specific transition temperatures (Ref. 2). Furthermore, space-exposed FEP can be eroded by atomic oxygen, which is formed in low Earth orbit (LEO) from the photodissociation of molecular oxygen by short wavelength energetic UV radiation. By Servicing Mission 2 (SM2, during STS-82), in February 1997, severe cracking of the 5 mil (127 μm) thick Al-FEP outer layer of the MLI blankets was observed on the light shield, forward shell and equipment bays of the HST (Refs. 3 and 4). The worst cracks in MLI on Equipment Bays 8 and 10 were covered during the mission with two patches of 2 mil (50.8 μm) thick Al-FEP on each bay (Fig. 1).

In May 2009 during the 5th servicing mission (called SM4, during STS-125), two degraded MLI blankets that were originally installed on the telescope and had 19 years of space exposure were replaced with new insulation pieces, called New Outer Blanket Layers (NOBLs). The space exposed MLI blankets were brought back for analyses by researchers at NASA Glenn Research Center and NASA Goddard Space Flight Center. No other spacecraft material has been retrieved and analyzed after having this length of space exposure. The two blankets retrieved during SM4 included Equipment Bay 8 MLI, which received direct sunlight, and Equipment Bay 5 MLI, which received grazing sunlight. Also retrieved were remnants of the two patches that were placed over cracked areas on Bay 8 during SM2 and were exposed to space for 12.3 years. The Al-FEP outer layers of the retrieved MLI blankets were found to be highly degraded, and have been analyzed for changes in optical, physical, and mechanical properties, along with space induced chemical and morphological changes and heat induced changes. This paper reviews the tensile and bend-test properties, density, thickness, solar absorptance, thermal emittance, x-ray

(a) (b)

Figure 1.—On-orbit photos of Equipment Bay 8 at SM2 (a) Before with cracked areas circled, and (b) After placement of the 2 mil Al-FEP patches.

photoelectron spectroscopy (XPS) and energy dispersive spectroscopy (EDS) elemental composition measurements, surface and crack morphologies, and atomic oxygen erosion values of the outer Al-FEP layer of the retrieved HST blankets after 19 years of space exposure.

2.0 Materials and Environmental Exposure

2.1 HST SM4 Bay 5 and Bay 8 MLI

The Bay 5 and 8 MLI blankets originally installed on HST (exposed to space for 19.1 years), and 2 mil Al-FEP patches installed on Bay 8 on February 18, 1997 during SM2 (exposed to space for 12.2 years) were retrieved by astronaut John Grunsfeld on May 18, 2009 during SM4, as shown in Figure 2. As can be seen in the illustration in Figure 3, Bay 8 is located 15° from the +V3 solar facing axis, and therefore is almost directly facing the sun. Bay 5 faces towards the +V2 solar array drive arm direction, and at 75° from the +V3 direction, receives grazing sunlight.

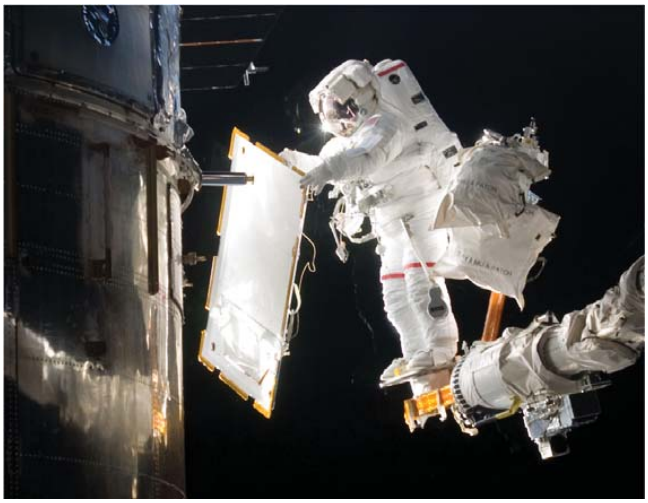

Figure 2.—Astronaut John Grunsfeld placing a NOBL on Bay 8 after he removed the damaged Bay 8 MLI and placed it folded into one of the EVA storage bags on his left along with the retrieved patch material. The second EVA bag contains the retrieved Bay 5 MLI blanket.

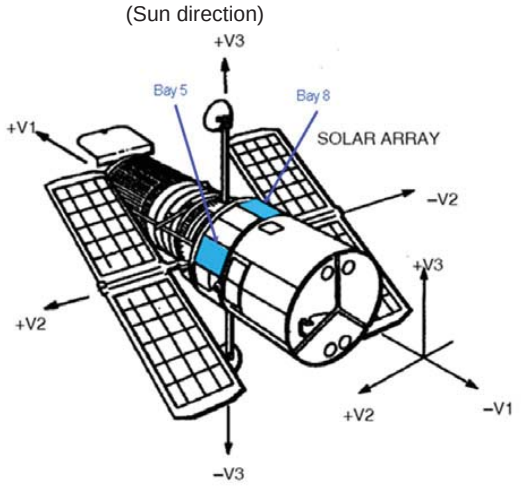

Figure 3.—Locations and orientations of Bays 5 and 8 on HST (+V3 is the solar facing axis).

2.2 Environmental Exposure

The sun exposure on each bay was determined by the science pointing profile of HST. The attitude profile between January 1, 2000 and SM4 was analyzed to determine the "typical" attitude of HST. The results were then extrapolated to provide estimates of the sun exposure since launch. Equivalent hours of sun exposure (ESH) of the telescope from deployment to SM4 are estimated as 111,000 hr, based on time in orbit, average time exposed to the sun per orbit, and length of each orbit. Based on the attitude profile from 2000 through SM4, and extrapolating over mission life, Bay 5 was exposed to ~24,300 ESH and the unpatched and patched areas of the Bay 8 MLI were exposed to ~89,300 and ~30,300 ESH, respectively.

The HST underwent an estimated 110,000 thermal cycles overall, from deployment to SM4. The range of temperatures seen by Bay 5 and Bay 8 vary greatly, because they are dependent on HST attitude and environmental heating variables. Thermal Desktop was used to model the Bay 5 and Bay 8 MLI and simulate the general thermal cycling behavior. Bay 5 MLI temperatures were estimated to range from –175 to 0 °C and the Bay 8 temperatures were estimated to range from –175 to 40 °C, for the attitude and orbit configurations modeled. A region of Bay 8 had been patched with a thin layer of Al-FEP in 1997, which resulted in decreased exposure to some space environmental effects such as radiation and atomic oxygen, but may have increased the maximum on-orbit temperature for the original top layer of the MLI blanket in that region. Additionally, a section of Bay 8 had undergone stress cracking causing a large piece to curl up while on orbit. This section may also have received higher maximum on-orbit temperatures than the flat regions of Bay 8 that remained intact and flat, while receiving some protection from radiation and atomic oxygen effects.

The X-ray fluence for solar facing surfaces was computed to be 641.1 J/m^2 between 1-8 Å and 43.1 J/m^2 between 0.5-4 Å. Data for x-ray fluence are based on x-ray flux data from the Geosynchronous Operational Environmental Satellites (GOES) for the time period of launch (April 1990) through SM2 (February 1997) (Ref. 5). For SM2 through SM4, the x-ray fluence was estimated assuming an average 11-year solar cycle (Ref. 5).

Electron and proton fluence from solar wind particles trapped in Earth's magnetic field have been calculated from deployment until December 9, 1999 using NASA's proton and electron models, AP-8 and AE-8, respectively (Ref. 5). The data for SM4 were extrapolated from these prior data, and indicated the Bay 5 and Bay 8 MLI received an electron fluence of 5.6×10^{13} particles/cm^2 for electrons >40 keV, and a proton fluence of 5.4×10^{10} particles/cm^2 for protons >40 keV.

The atomic oxygen fluence was computed for the duration of the HST mission over the period of time from deployment to SM4. This was accomplished by adding: (1) the prediction over the period of time from deployment to SM1 as predicted by SAIC's version 5.0 Environmental Work Bench, which uses MSIS-86 atmospheric model, to (2) a prediction based on orbital and atmospheric data from NASA Goddard for SM1 to SM4. The parameters used in the SM1 to SM4 fluence calculation included altitude, atmospheric density, and orbital velocity corrected for the Earth's atmosphere co-rotation. Based on these calculations the total ram fluence was 2.61×10^{21} atoms/cm^2. If the surfaces of Bay 8 are 15° from solar facing, then the fluence would be ~25.8 percent of the ram fluence or ~6.73×10^{20} atoms/cm^2. But, as the surfaces are solar facing but randomly tipped (always with Bay 8 somewhat towards the sun), then the fluence is decreased an additional factor of $2/\pi$ resulting in the probable fluence of ~4.28×10^{20} atoms/cm^2. Because the Bay 5 faces towards the +V2 direction and is 75° off the solar facing axis, the fluence was estimated as ~28.0 percent of the ram fluence, or 7.30×10^{20} atoms/cm^2. As the surfaces are randomly tipped, the fluence would be decreased by $2/\pi$ resulting in a probable fluence of ~4.65×10^{20} atoms/cm^2.

Environmental exposure for patched and curled regions was calculated based on the time periods when these regions were uncovered. The patches were assumed to protect a region until the midpoint between the last servicing mission when the patch was viewed covering the region and the first servicing mission when the region was observed unprotected. A table of the exposure values for all regions is provided in Section 4.1.

3.0 Experimental Procedures

3.1 Scanning Electron Microscopy

Either a Hitachi S-4700 field emission scanning electron microscopes (FESEM) operated at an accelerating voltage of 6 kV, or a Hitachi S-3500 operated at an accelerating voltage of 10 kV, were used at GRC to document various surface features, such as erosion morphologies, cracks and impact sites. The samples were sputter-coated with thin gold-palladium (Au-Pd) films to make them conductive for imaging. Energy dispersive spectroscopy (EDS) was conducted using either EDAX CDU Leap Detector or IXRF Detector systems.

3.2 Thickness Measurements

Thickness measurements were taken at three locations along the cross section of each sample, using a LEO Supra 50VP scanning electron microscope (SEM) at GSFC, with an accelerating voltage of 20 kev. Samples for SEM thickness measurements were mounted in epoxy, and then SiC paper and diamond slurry were used to polish the cross sections. These thickness measurements were used to calculate atomic oxygen erosion yield and bend-testing strain.

A Heidenhain MT12 drop gauge was used to measure the thickness of all regions at GRC. Thickness was measured in three locations on the grip area of each sample used for tensile testing (4 to 17 samples per region). These thickness measurements were used to determine cross sectional area individually for each sample when calculating tensile stress. The average thickness in each region was also used to calculate bend-test strain and atomic oxygen erosion yield. The drop gauge thickness measurements were used for these calculations because thickness was found to vary significantly within each region, and SEM measurements were only made at one or two locations within each region.

3.3 Tensile Properties

A DDL Inc. Model 200Q Electromechanical Test System was used to measure load and displacement during tensile elongation. From this data, the percent elongation at failure and ultimate tensile strength (UTS) were determined. The tensile samples were sectioned to the specifications defined in American Society for Testing and Materials (ASTM) Standard D-638 for Type V tensile specimens (Ref. 6). Care was taken to avoid cracks and impact sites. The initial sample length was set at 25.4 mm and the elongation rate was 12.7 mm/min. As an update from previously reported results of tensile testing SM4 material (Ref. 7), tensile stress was calculated based on the thickness of each sample individually measured using the Heidenhain drop gauge.

3.4 Bend-Testing

Bend-testing was conducted on samples from select regions to assess tensile strain induced surface cracking. The bend-test procedure induced a surface tensile strain without adding an overall tensile load to the samples. The strain necessary to induce surface cracking was determined by bending 1.3×0.5 cm samples over successively smaller mandrels until cracking was observed. The test apparatus used a pliable platform to push the samples against the mandrel without applying overall tension, as illustrated in Figure 4. Each sample was placed with the space-exposed surface face-down on the platform and then bent into a U-shape, with the space exposed surface on the outside under tension and the back surface under compression.

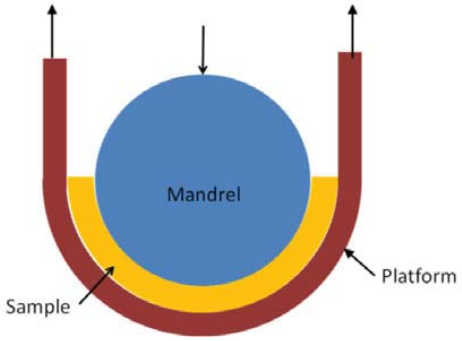

Figure 4.—Illustration of the bend-test configuration showing a cradle platform used to bend the sample around the mandrel.

Optical microscopy was used to document surface features in the bend-test area prior to testing, and the same area was examined after bending around each mandrel to identify and document any induced surface cracks. The samples were examined at magnifications up to approximately 50X with an Olympus SMZ stereo-zoom optical microscope outfitted with a Canon digital camera. This procedure was continued with samples bent around successively smaller mandrels until cracks were visible or until the sample did not experience any cracking with the smallest mandrel, in which case the sample was recorded as having not cracked. Samples were bent over up to 69 mandrels with diameters ranging from 1.253 to 0.052 cm in order of decreasing diameter (increasing tensile strain). The percent strain at failure, E, is given by

$$E = \left(\frac{t}{t+d} \right) \times 100 \tag{1}$$

where t is the thickness of the sample and d is the diameter of the mandrel that caused cracking. Sample thickness t was taken as the average of all drop gauge thickness measurements from that region. Bend-testing is well suited to very brittle material because no overall tension is applied to the samples and small strains can be accurately measured.

3.5 Density

Density was measured using calibrated density gradient columns. The density gradient was established in a 50 mL buret using two solutions of carbon tetrachloride (CCl_4, 1.594 g/cm^3) and bromoform ($CHBr_3$, 2.899 g/cm^3). A less dense solution (1.803 g/cm^3) was siphoned into a continuously stirred beaker initially containing only a more dense solution (2.299 g/cm^3), from which an equal flow was directed into the buret. Because the amount of lighter solution in the effluent from the beaker increased over time, solution density continuously decreased as a function of height. A quadratic calibration curve was developed for each column based on the equilibrium vertical position of three to four standards of known density (±0.0001 g/cm^3). Subsequently, density values were calculated from the vertical positions of small (< 2 mm) samples placed into the column and allowed to settle for 2 hr. Data were obtained from four separate density columns, with the density of each exposure region being measured at least twice. The very thin vapor-deposited aluminum backing on the FEP was previously determined to have no measureable effect on density measurements, and therefore was not removed prior to density measurements (Ref. 8).

3.6 Optical and Thermal Properties

Solar absorptance and thermal emittance measurements were taken at both GSFC and GRC. Cary 5000 spectrophotometers equipped with Spectralon integrating spheres were used to measure total reflectance from 250 to 2500 nm at an 8° angle of incidence at both locations. Absorptivity data were integrated with respect to the air mass zero solar spectrum to obtain solar absorptance. Samples at GRC were measured with an Al spacer backed by a single layer of sample of the quilted Al/Kapton/Al inner film (Region 8.15) replicating the on-orbit configuration.

Emissivity measurements were obtained at GSFC using a Gier-Dünkle DB-100 InfraRed Reflectometer following the ASTM E408-71 standard test method. The normal emittance (ε_n) of the surface was measured from 5 to 40 μm while at room temperature. Three measurements were taken for each sample, with the exception of Bay 8 Region 3, which was highly delaminated, hence only one measurement was taken. Emissivity measurements were obtained at GRC using a Surface Optics Corporation Model SOC 400T Reflectometer. The SOC 400T measures the directional reflectance of surfaces over a large spectral range, 2 to 25 μm, to obtain the directional thermal emittance over a large temperature range. Automatic integration of reflectivity data in the infrared with respect to blackbody curves is used to calculate total emittance for a selectable temperature range. Data were obtained at 293, 313, and 393 K. The samples were placed in the sample holder face-down with an aluminum spacer and were backed by a sample of the quilted Al/Kapton/Al MLI inner layer.

3.7 Atomic Oxygen (AO) Erosion Yield (Ey)

The volume eroded per incident atomic oxygen atom (cm^3/atom), or erosion yield (Ey), of the HST samples was calculated in two distinct ways, by mass loss and by thickness loss. Some of the HST material experienced a density change on orbit, so part of the observed thickness loss was caused by the density change, not atomic oxygen erosion. Therefore, while erosion yield can typically be calculated simply by dividing thickness loss by atomic oxygen fluence, in this case it was calculated using the following Equation (2)

$$\mathrm{Ey} = \frac{t_i - t_f \rho_{f/} \rho_i}{F} \tag{2}$$

where t_i is the thickness of pristine material, t_f is the thickness of the space-exposed material, ρ_i is the density of pristine material, ρ_f is the density of the space-exposed material, and F is the atomic oxygen fluence (atom/cm^2). In this equation, the numerator represents the thickness loss that can be attributed to AO erosion. This calculation is an update from previously reported atomic oxygen erosion yield data for the Bay 5 and Bay 8, which was calculated assuming constant density (Ref. 7).

To determine mass loss Ey, the mass of 12.7 mm diameter circular samples were measured using a Mettler M3 balance and compared to the mass of pristine material. Mass loss Ey was calculated using the following Equation (3)

$$\mathrm{Ey} = \frac{\Delta M}{\rho_i A F} \tag{3}$$

where ΔM is the measured mass loss and A is the exposed surface area of the sample. The result of this expression is directly comparable to Ey calculated using Equation (3).

3.8 X-ray Photoelectron Spectroscopy (XPS)

Samples were analyzed for elemental composition using a M-Probe X-Ray Photoelectron Spectrometer. Three locations on samples from various regions were run using a general survey scan, with a spot size of 800 μm, to determine atomic percent composition.

3.9 Static Heat Treatment

The solar absorptance, thermal emittance, tensile properties, and density of heat treated samples were measured in addition to the as-retrieved material. Density measurements were taken after both 120 and 200 °C heat treatments. A heat treatment at 200 °C was used for tensile strength samples and a heat treatment at 120 °C was used for solar absorptance and thermal emittance samples. Heating at 200 °C corresponds to the maximum temperature experienced on-orbit by very tightly curled insulation (Refs. 4 and 5). The 120 °C treatment was chosen to represent a more moderate on-orbit heating condition. Heating was conducted in air for 96 hr as prior data indicate a minimum of 72 hr is necessary for heating effects to be stabilized (Ref. 8). Bend-tests of the 200 °C heated HST material were planned but not completed because the insulation curled significantly on heating.

4.0 Results and Discussion

To retrieve the MLI blankets, astronaut John Grunsfeld unpeeled each blanket from its Velcro secured border, then folded the blankets and placed them into EVA storage bags (Fig. 2). Although great care was taken in retrieval planning and execution, the retrieval process did cause cracking at fold seams, introducing handling cracks that were not present on-orbit prior to retrieval.

The Bay 5 and Bay 8 MLI blankets are shown in the on-orbit photos taken during SM4 in Figures 5(a) and (b), respectively. The Bay 5 MLI has several large cracks extending from the two rectangular radiator areas. The Bay 8 MLI also has several very large cracks, and one side of the largest crack on Bay 8 curled up into a cone-like roll, as seen in Figure 5(b). Also, the Bay 8 patches were highly degraded with the majority of the Al-FEP completely gone. Upon post-retrieval visual inspection, the Bay 8 MLI appeared significantly more degraded than the Bay 5 MLI, as the Bay 8 MLI had broken into many fragments after removing it from the EVA bag, unfolding it and laying it flat again. In fact, the Bay 8 Al-FEP outer layer needed to be reassembled post-flight like a jigsaw puzzle.

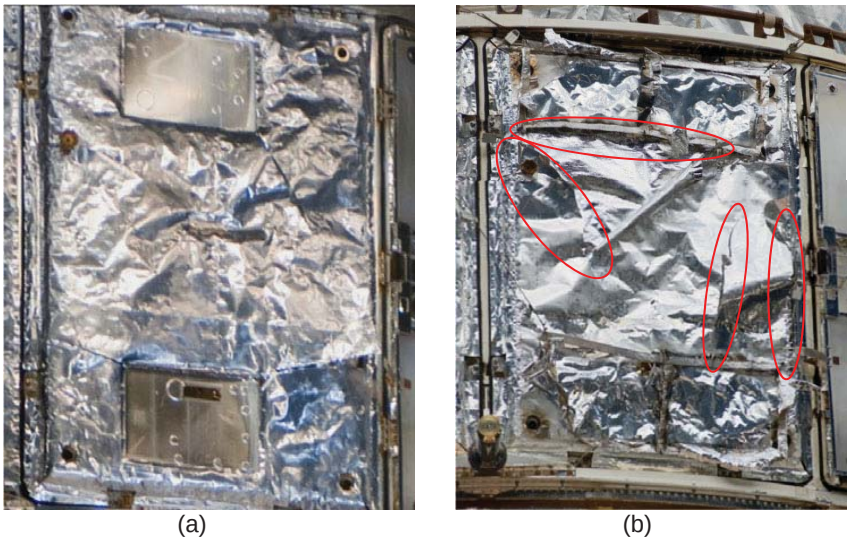

(a) (b)

Figure 5.—On-orbit photos of Equipment Bays 5 and 8 just prior to retrieval during SM4: (a) Bay 5, and (b) Bay 8 with large cracks circled.

4.1 Exposure Regions

The retrieved Bay 5 and Bay 8 MLI blankets contained a range of unique regions that were identified based on environmental exposure and/or physical appearance and assigned numbers. For example, the Bay 8 MLI that was not covered by patch material and was exposed to the space environment for the full 19.1 years had areas with three distinct appearances: shiny areas ("nominal"), hazy-white areas and areas where the Al was delaminated. These regions were defined as Regions 8.1, 8.2 and 8.3 (R8.1, R8.2 and R8.3), respectively. Examples of these regions are provided in Figure 6. Also, as mentioned, one of the Bay 8 outer layer Al-FEP cracked areas (not covered by patch material) curled up into a cone-like roll. In the curled region, the backside Al was exposed to the space environment. This material was heated to a higher temperature on-orbit than the nominal space-facing FEP because of the lower emittance of the aluminized surface. The curled area was divided into two regions: a tightly curled region (R8.7) and a loosely curled region (R8.8), as those two regions may have heated differently on-orbit. This curling was not observed at SM3B, so the insulation was in the curled state for no more than 7.1 years. Some areas of the patches installed during SM2 eventually degraded exposing the underlying MLI to the space environment once again as observed during SM3B and SM4. Therefore, the MLI under the patched areas is divided into two regions: the region patched during SM2 and exposed by SM3B (SM2-SM3B, patched 5.1 years, called R8.13), and the region patched during SM2 and still covered at SM4 (SM2-SM4, patched 12.2 years, called R8.11).

A total of 10 different regions were identified on Bay 5 (R1-R10), and 15 different regions were identified on Bay 8 (R1-R15) and 4 regions identified on the retrieved Patches (R16-R19). The regions selected for testing are defined in Table 1 and shown in Figure 7. During sectioning of samples from the blankets, care was taken to avoid any cracks or imperfections in the samples which would affect the tests.

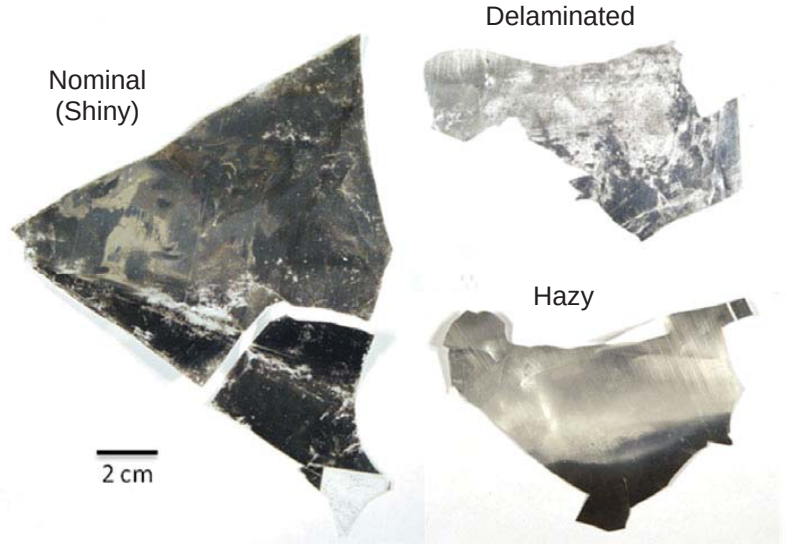

Figure 6.—Bay 8 nominal (shiny), hazy and delaminated MLI fragments.

TABLE 1.—HST SM4 BAY 5 AND BAY 8 REGION DEFINITIONS AND ENVIRONMENTAL EXPOSURES

HST Material Bay.Region	Description	AO Fluence (E+20 atom/cm^2)	Equivalent Sun Hours	Max. On-Orbit Temp (°C)*	Proton Fluence (E+10 particles /cm^2)	Electron Fluence (E+13 particles /cm^2)	X-ray Fluence (J/cm^2)	
							1-8 Å	0.5-4 Å
Pristine (P)	Pristine 5 mil Al-FEP	-	-	-	-	-		-
5.1	Nominal/Shiny	4.65	24,300	0	5.4	5.60	641.1	43.1
5.4	Nominal/Al-Delaminated	4.65	24,300	0	5.4	5.6	641.1	43.1
8.1	Nominal/Shiny	4.28	89,300	40	5.4	5.6	641.1	43.1
8.2	Nominal/White Hazy	4.28	89,300	40	5.4	5.6	641.1	43.1
8.3	Nominal/Al-Delaminated	4.28	89,300	40	5.4	5.6	641.1	43.1
8.7**+	Cone/ Tight Curl	3.92	72,400	>120 <200	4.4	4.5	519.8	34.9
8.8**+	Cone/ Loose Curl	3.92	72,400	>120 <200	4.4	4.5	519.8	34.9
8.11**+	Patched SM2-SM4	1.64	30,300	>40 <120	1.8	1.9	217.5	14.6
8.13**+	Patched SM2-SM3B	2.69	70,800	40	4.3	4.4	508.3	34.2
8.15	Protected Inner Layer (Al/Kapton/Al)	-	-	-	-	-	-	-

* All HST material had 110,000 total thermal cycles and a minimum temperature of –175 °C

** Proton, electron, and x-ray fluences for these regions were calculated assuming constant flux over the exposure period of the insulation.

\+ Temperature ranges for these regions were determined based on density measurements of as-retrieved and ground-heated samples (see section 4.5).

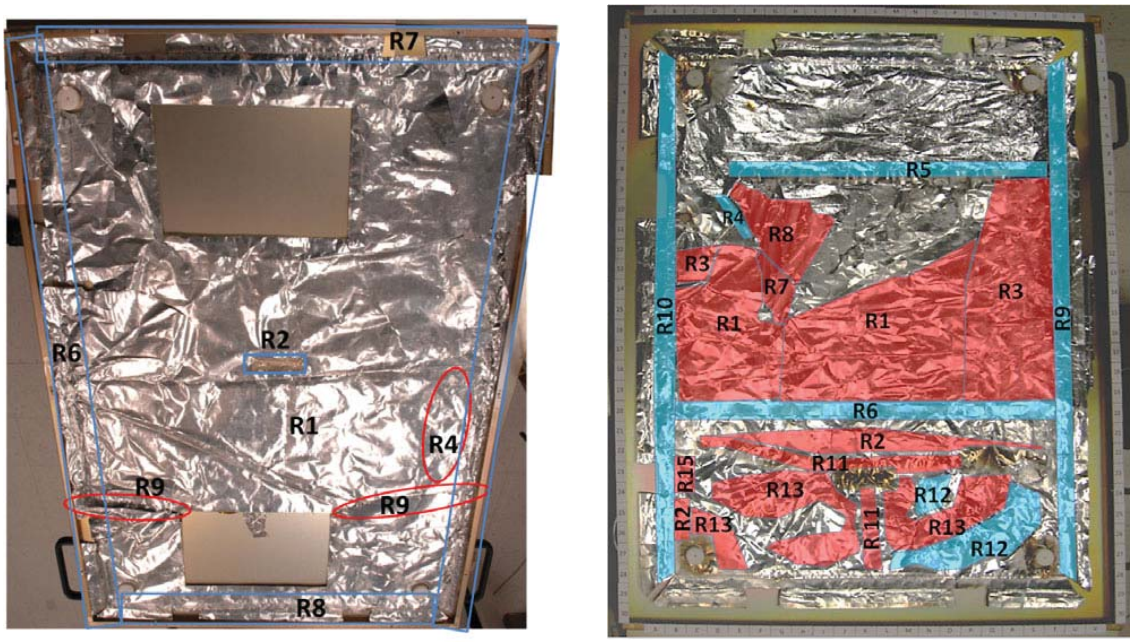

(a) (b)

Figure 7.—Photographs of Bay 5 and Bay 8 with exposure regions identified: (a) Bay 5, and (b) Reassembled Bay 8 (red regions were tested, blue regions were not).

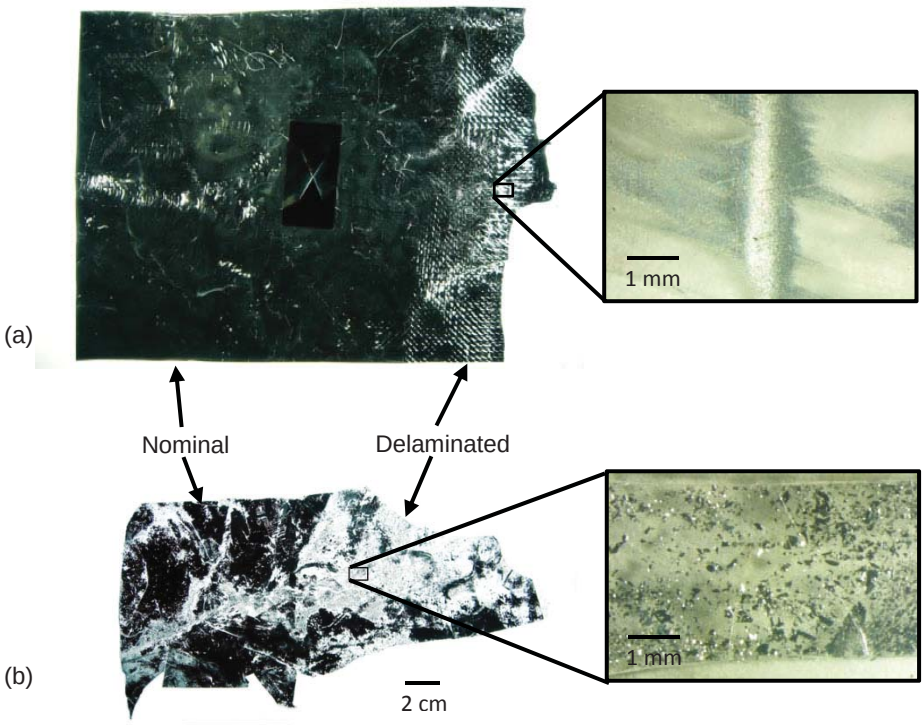

Figure 8.—Comparison of Bay 5 and Bay 8 shiny and delaminated regions: (a) A section of material cut from Bay 5, and (b) A cracked fragment of Bay 8 material (back lit photos).

The delaminated regions of Bay 5 and Bay 8 have very different physical appearances; therefore the delamination may not have been caused by the same factor. Bay 5 delaminated samples (an example is provided in Fig. 8) have a checkerboard-like pattern of delaminated areas on a surface with predominately retained Al backing. There is no tendency for more Al to flake off. In contrast, Bay 8 delaminated samples (an example is provided in Fig. 8) have small patches of Al distributed throughout a mostly delaminated surface and additional Al easily spalls off from the FEP on handling the samples.

4.2 Scanning Electron Microscopy

Figures 9 and 10 compare the space-exposed (FEP) surfaces of Bay 8 Region1 (nominal/shiny) and Bay 8 Region 2 (nominal/hazy) using the Hitachi S-4700. Atomic oxygen erosion has resulted in distinct textures in these two regions. The shiny material has fine, rill-like directional texturing, whereas the hazy material has larger rounded features. The difference in texture may be attributed to the hazy region being located near the top edge of the bottom patch, where it may have received additional shadowing and/or scattering of AO from the patch at various times in the orbit. EDS spectra of Regions 1 and 2 are shown in Figures 11(a) and (b), respectively. The spectra indicate that only C and F peaks, and very small Au and Pd peaks from the Au-Pd conductive coating, are present. There is no presence of Si, hence no indication of silicone contamination in the nominal/shiny region, nor in the hazy region. However, a barely detectable Si peak was detected on a Bay 8 Region 1 sample imaged with the Hitachi S-3500. Figure 12 shows the space-exposed (FEP) surface of Bay 8 Region 3 (delaminated). The FEP is clearly cracked in the delaminated region, and the texture appears to be less pronounced as compared to Regions 8.1 and 8.2. It is not known if the cracking occurred on-orbit or due to retrieval handling. The space-exposed FEP from Bay 8 Regions 7 and 11, and Bay 5 Region 1, are shown in Figures 13 to 15, respectively. Bay 8 Region 7, which became tightly curled on-orbit, looks similar in texture to Bay 8 Region 1 surfaces, with perhaps slightly less texture. The Bay 8 Region 11 surface, which was patched

between SM2-SM4, has more rounded rill features, possibly due to receiving scattered AO from the patch. Both these surfaces had barely detectable Si peaks. As can be seen in Figure 15, the Bay 5 Region 1 surface has a different appearance than the Bay 8 surfaces. Whereas the Bay 8 surfaces eroded with a texture consistent with receiving grazing, or sweeping, AO exposure, the Bay 5 Region 1 surface showed little evidence of erosion with no notable erosion texture. This is consistent with thickness measurements, discussed later, which indicate that the Bay 5 material was eroded the least. The Bay 5 surface did show a larger Si EDS peak, indicating that there is some silicone contamination on this surface. This is consistent with the XPS analyses reported later.

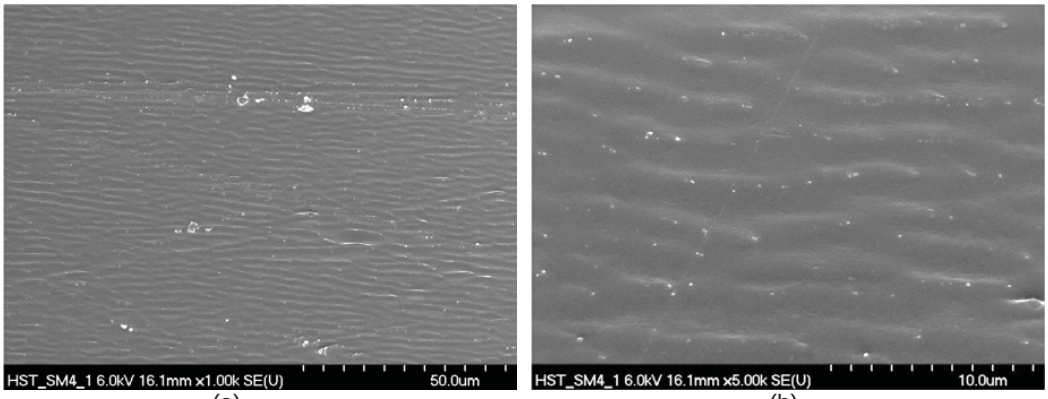

(a) (b)

Figure 9.—Space exposed FEP surface of Region 8.1 (nominal/shiny): (a) 1KX magnification (45° tilt), and (b) 5KX magnification (45° tilt).

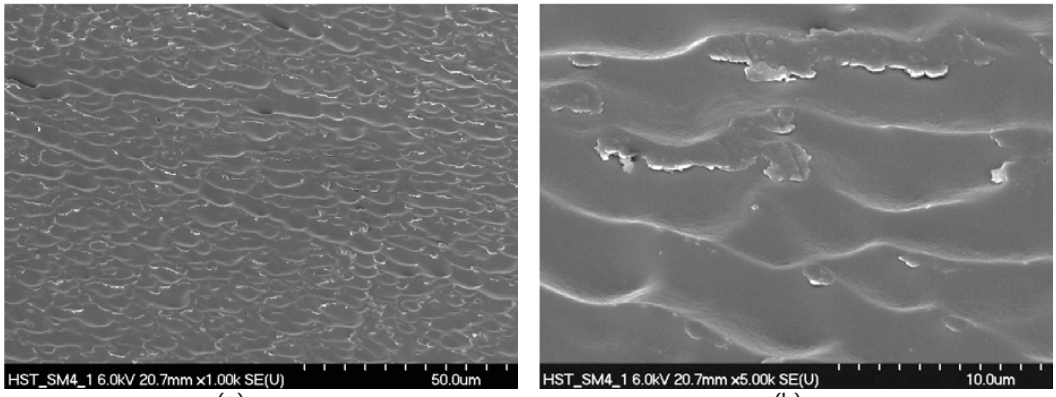

(a) (b)

Figure 10.—Space exposed FEP surface of Region 8.2 (hazy): (a) 1KX magnification (45° tilt), and (b) 5KX magnification (45° tilt).

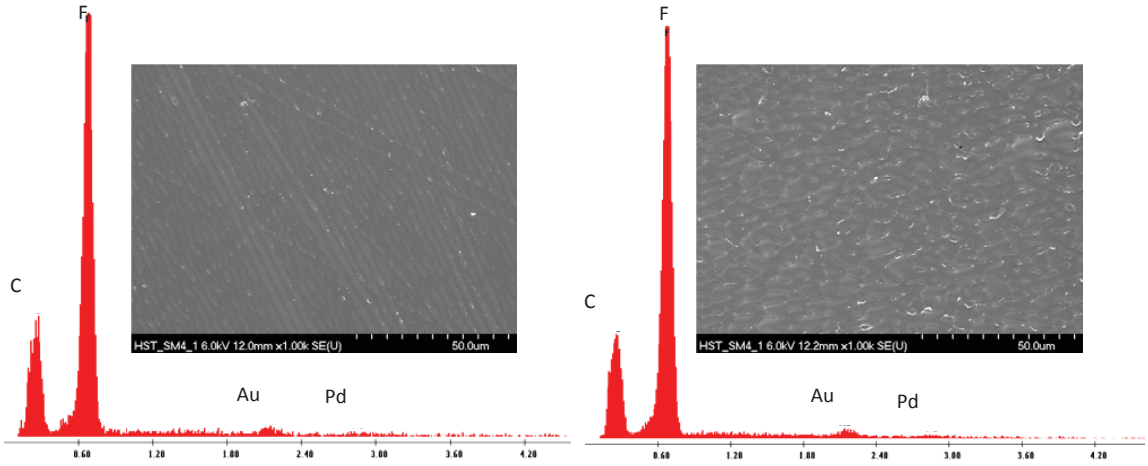

(a) (b)

Figure 11.—EDS spectra and corresponding SEM image areas (0° tilt) of space exposed Teflon FEP surfaces: (a) Region 8.1 Nominal/Shiny, and (b) Region 8.2 Hazy.

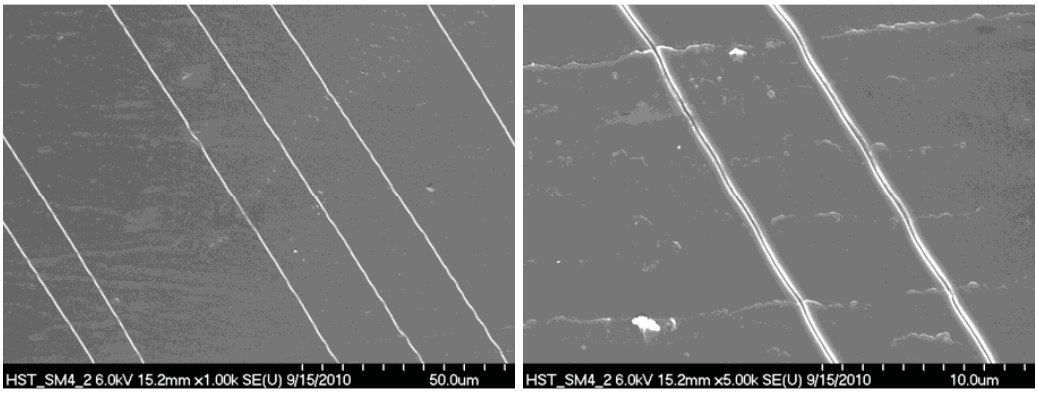

(a) (b)

Figure 12.—Space exposed FEP surface of Region 8.3 (delaminated): (a) 1KX magnification (0° tilt), and (b) 5KX magnification (0° tilt).

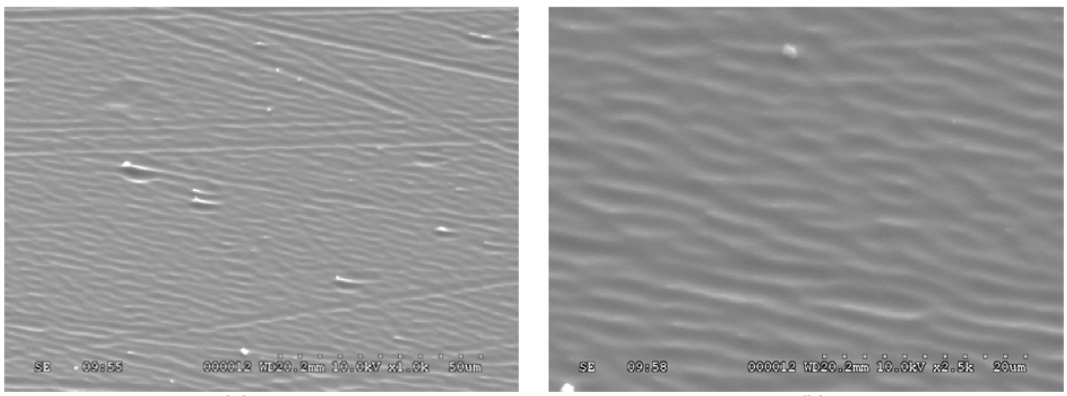

(a) (b)

Figure 13.—Space exposed FEP surface HST SM4 Region 8.7 (tightly curled region): (a) 1KX magnification (45° tilt), and (b) 2.5 KX magnification (45° tilt).

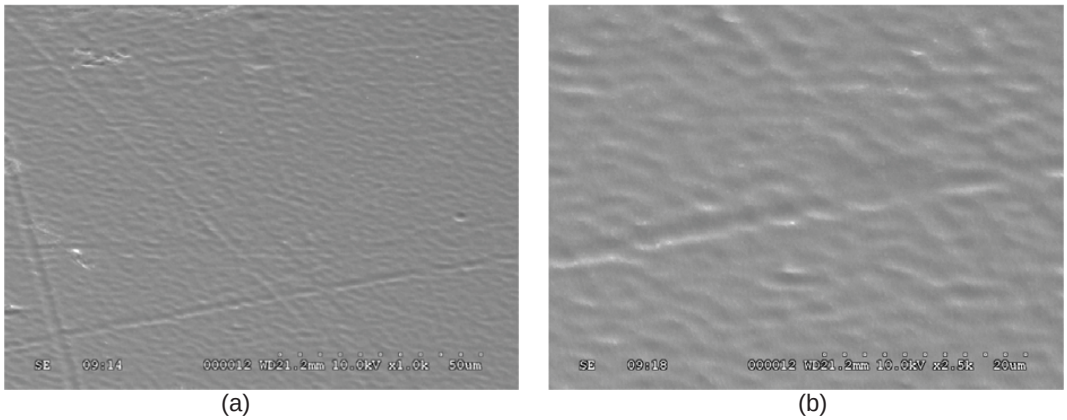

(a) (b)

Figure 14.—Space exposed FEP surface HST SM4 Region 8.11 (patched SM2-SM4): (a) 1KX magnification (45° tilt), and (b) 2.5 kX magnification (45° tilt).

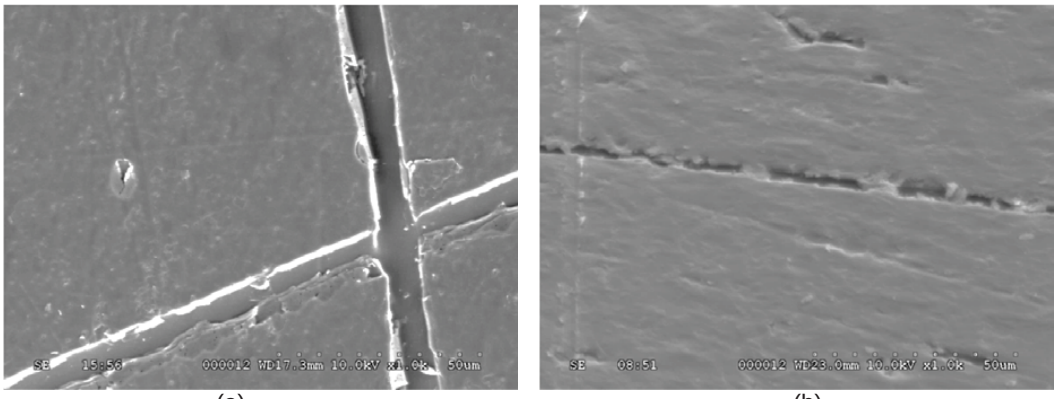

(a) (b)

Figure 15.—Space exposed FEP surface of Region 5.1 (nominal/shiny): (a) 1KX magnification (0° tilt), and (b) 1KX magnification (45° tilt).

Figures 16 to 18 compare the aluminum surfaces of pristine Al-FEP, Bay 8 Region1 (nominal/shiny) and Bay 8 Region 2 (nominal/hazy) materials, respectively. The aluminum surface of the pristine Al-FEP is smooth with no cracks, as shown in Figure 16(a). At very high magnification (100KX) a grain structure can be seen as shown in Figure 16(b). As can be seen in Figures 17(a) and 18(a), the aluminum layer of the HST material is cracked, with more cracks (smaller islands) present in the hazy region (18a). Cracking of the Al layer can be attributed to the stress caused during thermal cycling because of the difference in the coefficient of expansion between Al and FEP (Ref. 4). Another interesting observation is the apparent growth of microscopic crystals in the aluminum surface, as shown in Figures 17(b) and 18(b), as compared to the pristine Al-FEP in Figure 16(b).

Images of the aluminum backing of Bay 8 Region 7, Bay 8 Region 11 and Bay 5 Region 1 are shown in Figures 19(a) to (c), respectively. The Bay 8 Region 7 surface has more mud-tiling than Bay 7 Region 1, and appears similar to the extent of mud-tiling of Bay 8 Region 2. The Bay 8 Region 11 surface, patched between SM2 and SM4, had the most extensive, finiest, mud-tiling. It was determined that this region received a higher temperature on-orbit with the patch in place. Bay 8 Region 7 also experienced a higher temperature on-orbit, but the curling was estimated to begin after SM3B, and hence had excessiving heating for a maximum of 7.1 years, and the tightly curled region would have been heated the least (at the bottom of the curled region). Bay 8 Region 11 would have received intense heating for approximately 12.2 years. The Al backing of the Bay 5 Region 1 material had more mud-tiling compared to Bay 8 Region 1. It appeared similar to the extent of mud-tiling of Bay 8 Region 2 or Bay 8 Region 7. The maximum on-orbit temperature of the Bay 5 Region 1 MLI was estimated to be less (0°) than that of the Bay 8 Region 1 MLI (40°), so the extent of mud-tiling is not easily explained.

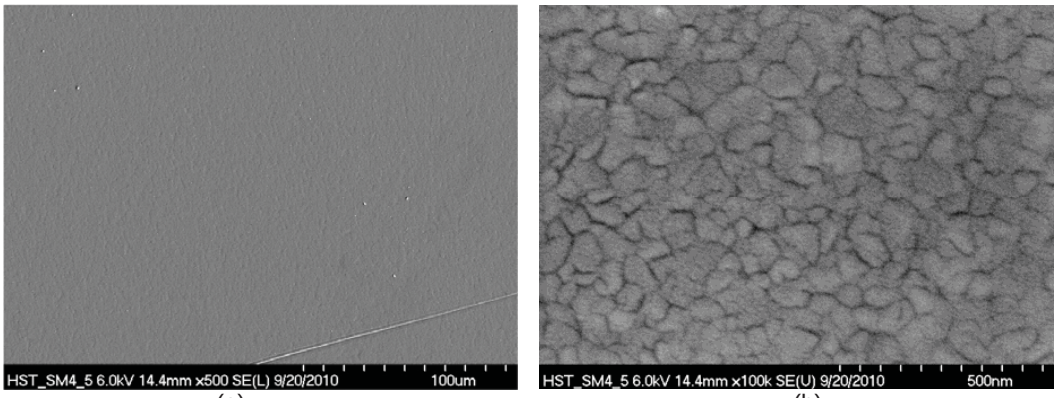

(a) (b)

Figure 16.—Aluminum backing of pristine Al-FEP: (a) 500X magnification (0° tilt), and (b) 100KX magnification (0° tilt).

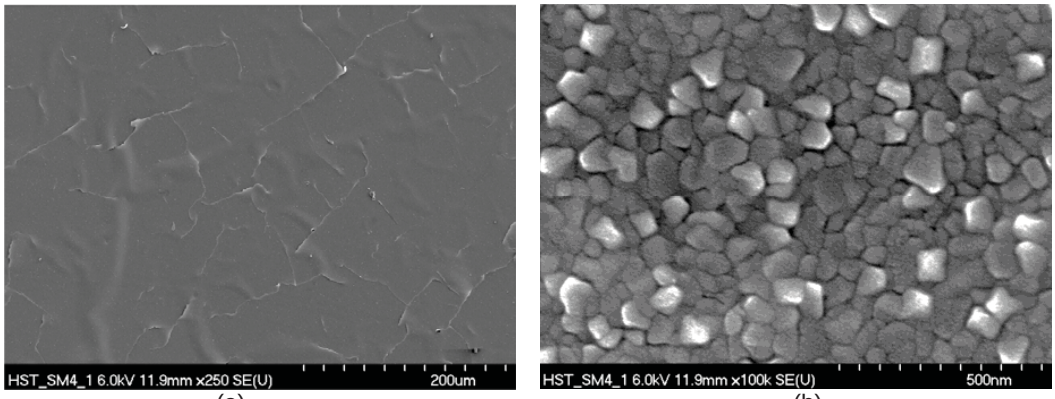

(a) (b)

Figure 17.—Aluminum backing of HST SM4 Region 8.1 (nominal/shiny): (a) 250X magnification (0° tilt), and (b) 100KX magnification (0° tilt).

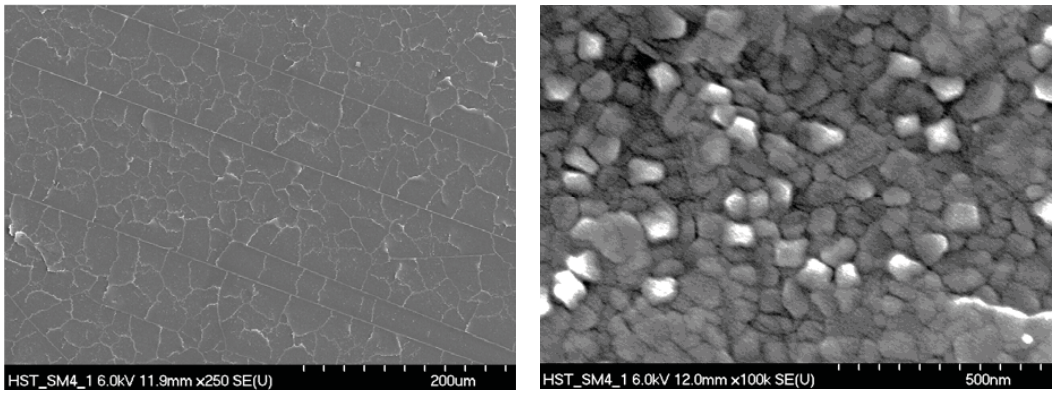

(a) (b)

Figure 18.—Aluminum backing of HST SM4 Region 8.2 (hazy): (a) 250X magnification (0° tilt), and (b) 100KX magnification (0° tilt).

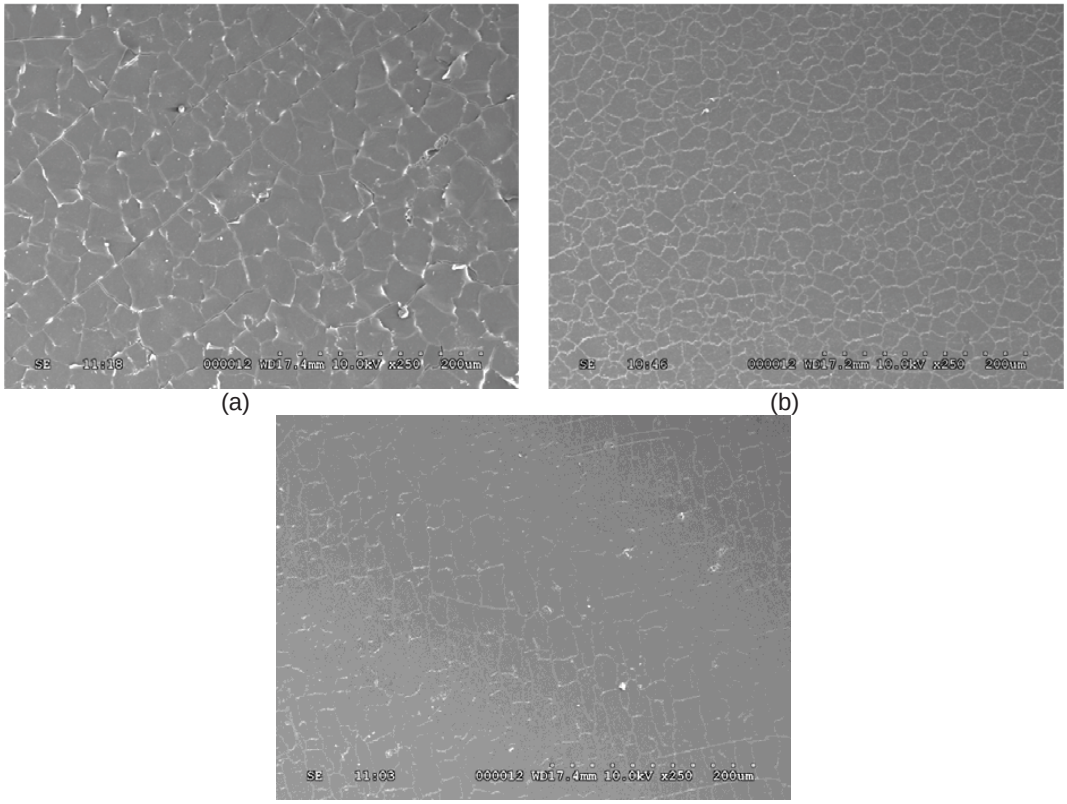

Figure 19.—Aluminum backing (250X, 0° tilt) of: (a) HST SM4 Region 8.7 (tightly curled region), (b) HST SM4 Region 8.11 (patched SM2-SM4), and (c) HST SM4 Region 5.1 (nominal/shiny).

Several micrometeoroid and orbital debris (MMOD) impact sites were observed on the HST material. A typical impact site is shown in Figure 20, with fine cracking of the FEP layer visible near the impact site.

SEM micrographs show very clear differences in the morphologies of on-orbit formed cracks (Fig. 21) and post-flight handling formed cracks (Fig. 22). Handling cracks have fibrous features typical of ductile failure. However, the fracture surfaces of on-orbit cracks were very smooth. Similar observations were made on material retrieved during SM2, and this supports a slow crack growth mechanism in which on-orbit fractures propagate slowly under relatively low stresses, influenced by radiation and thermal cycling (Ref. 4).

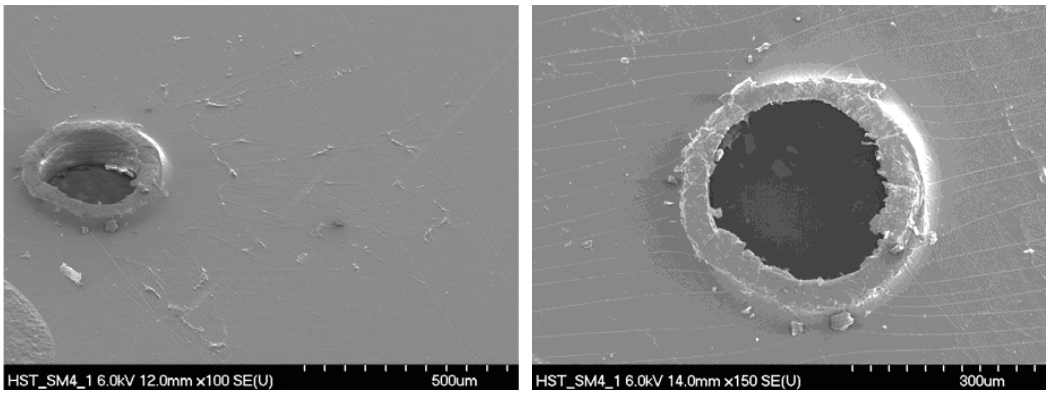

Figure 20.—An MMOD impact site in Bay 8 Region 1.

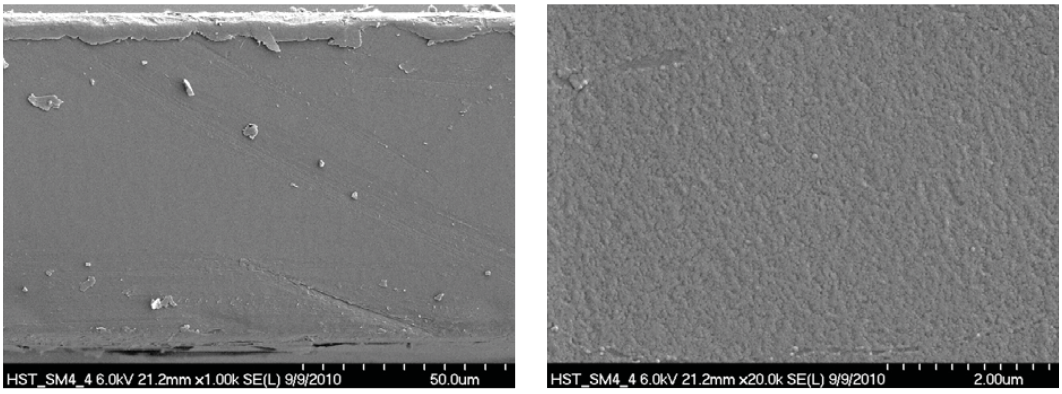

(a) (b)

Figure 21.—Edge on view of an on-orbit formed crack in HST SM4 Region 8.1 FEP (nominal/shiny) showing a smooth texture: (a) 1KX magnification, and (b) 20KX magnification.

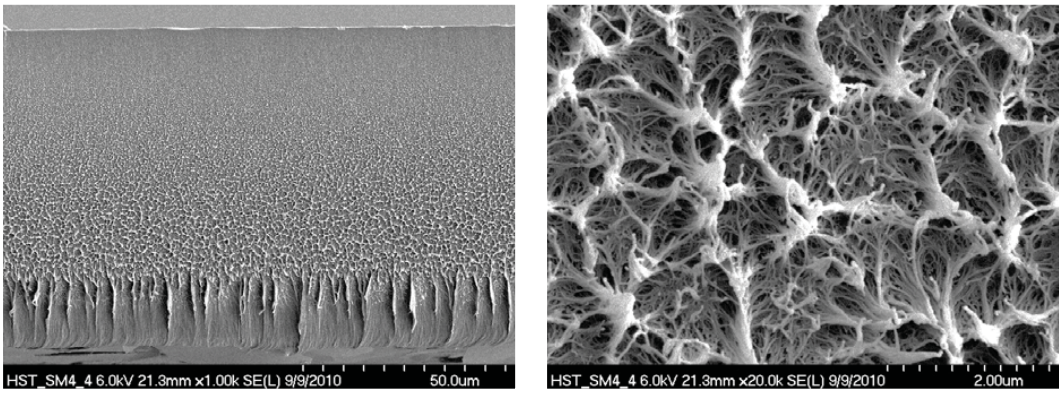

(a) (b)

Figure 22.—Edge on view of a post-flight handling formed crack in HST SM4 Region 8.1 FEP (nominal/shiny) showing a fibrous texture: (a) 1KX magnification, and (b) 20KX magnification.

4.3 Thickness Measurements

Thickness measurements from the SEM and drop gauge were largely similar, as shown in Table 2. However, thickness measurements using the drop gauge showed significant variability across different locations in a given region. The drop gauge measurements are better represent each region's over all thickness because thickness measurements were taken at many more locations within each region, as indicated in the table under the number of samples tested.

4.4 Tensile Properties and Bend-Test Results

The average ultimate tensile strength (UTS) and percent elongation at failure of the HST and pristine Al-FEP are provided in Table 3 and graphed in Figure 23. Because of the degree of embrittlement of the HST samples, many broke while being punched out or handled prior to testing. Others were tested but failed at pre-existing cracks, causing a premature break. Data from premature breaks were not included in the average. Five samples from Region 8.7 (tightly curled region) were tested, and all broke prematurely, thus no data are reported. For all other regions, usable data was obtained from 3 to 8 samples depending on material availability.

All HST material was extremely embrittled. Elongation at failure was reduced from 255 percent for pristine material to 8.5 percent for Bay 5 nominal/shiny material and to 1.5 percent for Bay 8 nominal/shiny material. The Bay 8 Al-FEP, which had a significantly higher solar exposure and on-orbit thermal cycling temperature, was found to fracture very easily with handling, like thin brittle glass. All regions also experienced large decreases in UTS, from 22.4 MPa for pristine Al-FEP to 13.3 and 5.9 MPa for Bay 5 and Bay 8 nominal/shiny material, respectively. Although the standard deviation is large compared to some of the absolute values, both the UTS and the elongation at failure appear to correlate with the amount of solar exposure received. For example, the solar facing Bay 8 material is more embrittled than the solar grazing Bay 5 material, and the elongation at failure of Bay 8 material is proportional to the amount of time that it was patched.

The decrease in both elongation and UTS indicates that the material has undergone significant scission of the polymer bonds. If the material had cross-linked with space irradiation, then the material should have experienced increased strength with the decreased elongation, which it did not experience.

TABLE 2.—COMPARISON OF DROP GAUGE AND SEM THICKNESS MEASUREMENTS*

HST Material Bay.Region	Drop Gauge (GRC)			SEM (GSFC)		
	No. of Samples	Avg. Thickness (μm)	Std. Dev. (μm)	No. of Samples	Avg. Thickness (μm)	Std. Dev. (μm)
Pristine	5	125.6	1.2	1	130.77	3.15
5.1	8	120.6	5.8	1	124.13	3.06
5.4	6	104.4	15.4	0	-	-
8.1	17	75.9	3.3	1	72.19	0.18
8.2	8	88.1	15.7	1	88.61	0.36
8.3	9	73.6	4.1	2	75.40	2.01
8.7	5	77.1	3.5	1	84.49	1.13
8.8	5	76.8	3.0	3	83.00	3.03
8.11	4	109.3	1.8	2	110.58	2.25
8.13	5	82.4	3.8	1	94.80	3.08

*For both techniques, thickness measurements were made three times on each sample.

TABLE 3.—TENSILE PROPERTIES OF PRISTINE AND HST Al-FEP

HST Material Bay.Region	No. of Samples Tested	No. of Cracked Samples Excluded	Avg. Thickness (μm)	Ultimate Tensile Strength		Elongation at Failure	
				Avg. (MPa)	Std. Dev.	Avg. (%)	Std. Dev.
Pristine (P)	13	0	125.6	22.4	0.8	254.7	9.7
P-200 °C	8	0	125.6	21.0	1.6	253.6	20.3
5.1	8	1	120.6	13.3	1.0	8.5	8.9
5.1-200 °C	8	1	123.0	9.4	1.9	2.3	0.3
5.4	6	2	104.4	9.5	2.0	2.3	0.4
8.1	17	5	75.9	5.9	1.5	1.4	0.3
8.2	8	3	88.1	8.9	3.5	2.7	0.9
8.3	9	4	73.6	8.4	3.5	2.4	1.1
8.7	5	5*	-	-	-	-	-
8.8	5	2	76.8	6.0	3.2	1.8	1.4
8.11	4	0	109.3	9.9	1.2	2.6	0.4
8.13	5	1	82.4	6.9	0.9	1.7	0.2

*All five samples broke prematurely, hence there is no tensile data

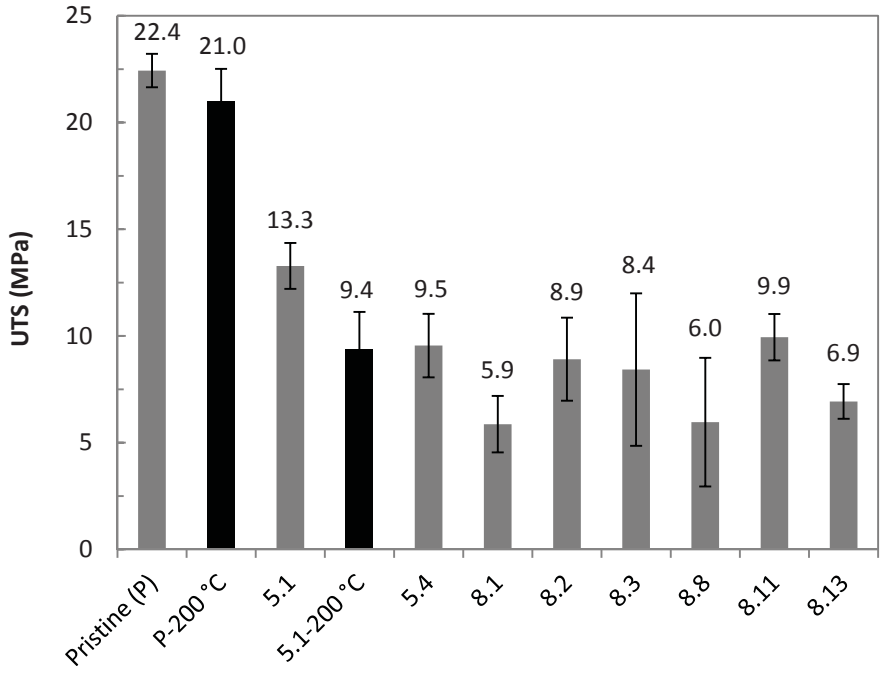

(a)

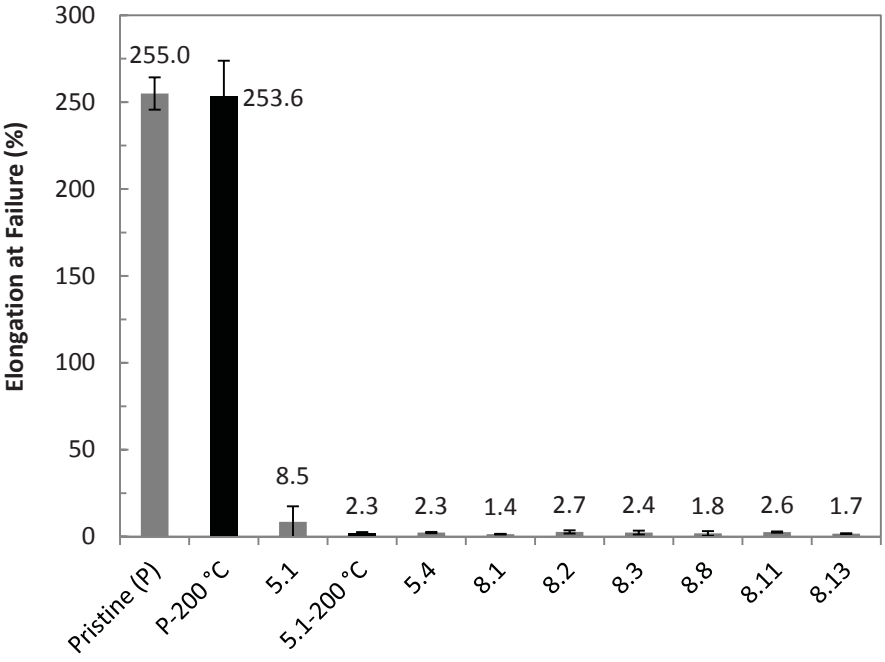

(b)

Figure 23.—Tensile properties of pristine and HST Al-FEP: (a) Average UTS and (b) Average elongation at failure.

TABLE 4.—COMPARISON OF ELONGATION AT FAILURE (*E*) FOR BEND AND TENSILE TESTS

HST SM4 Material Bay.Region	Bend-Test		Tensile Test	
	Number of Trials	Avg. *E* (percent)	Number of Trials	Avg. *E* (percent)
Pristine	1	No Failure*	8	255
5.1	3	6.69	7	8.51
8.1	3	0.82	12	1.51

*The maximum strain tested was 19.7 percent.

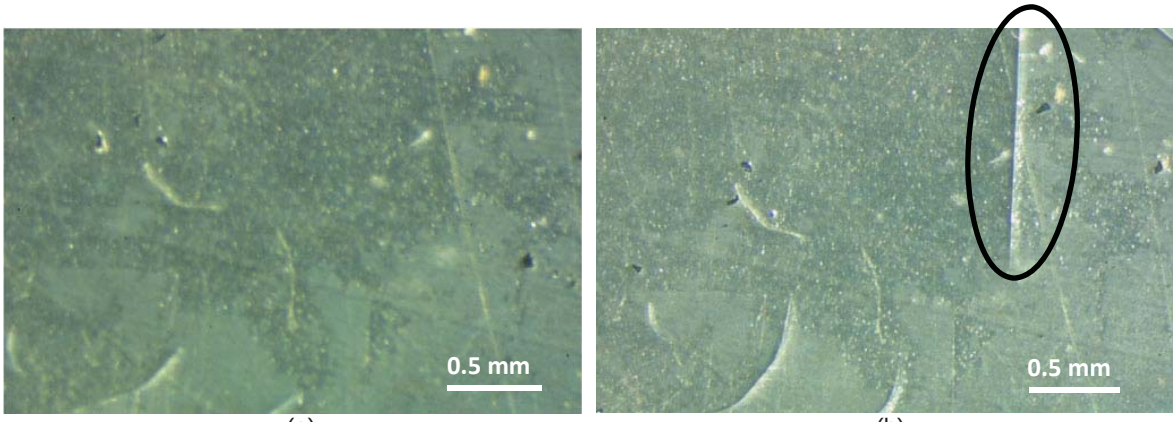

(a) (b)

Figure 24.—A sample from Bay 5 Region 1 (a) before and (b) after bend-testing with the bend-test-induced crack circled.

Heating pristine Al-FEP marginally decreased its strength and had no effect on elongation. The Bay 8 MLI was too embrittled to conduct studies to assess the effect of heating, but heating Bay 5 Region 1 material at 200 °C for 96 hr further reduced both the elongation and strength of the samples. This supports the mechanism proposed for degradation in which solar radiation and solar heating play synergistic roles.

To determine whether space-exposed Al-FEP continues to degrade after being returned to Earth, 11 samples from Bay 8 Region 1 were tested one year after recovery in 2010 and 6 samples were tested four years after recovery in 2013. There was no significant difference between these samples, so the results were combined.

The elongation at failure measured by bend-testing is shown and compared to the results of the tensile data in Table 4. Because bend-testing is designed for brittle samples, the maximum strain applied in the bend-test was insufficient to cause failure in pristine material. The elongation at failure measured by bend-testing qualitatively agrees with elongation at failure measured by tensile testing, with Bay 8 nominal material much more embrittled than Bay 5 nominal material. Therefore, bend-test results also support the conclusions from tensile testing. However, elongation at failure measured by bend-testing is slightly lower than elongation at failure measured by tensile testing. This discrepancy likely occurs because failure is defined as initial cracking for bend-testing, but it is defined as a complete break for tensile testing. A representative image of bend-test induced cracking failure is shown in Figure 24. Bend-tests to verify the effect of heating on Bay 5 Region 1 and Bay 8 Region 1 were not run because all samples curled significantly while being heated, which would affect the strains induced during testing.

Due to the brittle properties of the MLI and the high incidence of cracking, the data for Regions 5.1, 8.1, 8.11 and pristine Al-FEP were supplemented with microscale mechanical testing at GSFC. Microscale mechanical testing uses very small specimen sizes and offers the advantage that pre-existing macroscale cracks in the material do not promote premature failure of the specimen. These test specimens could experience strains and ultimate loads reflective of the environmental degradation seen in the material properties; however, the microscale test results are less conservative than traditional mechanical testing in that they do not account for the macroscale defects such as tears or cracks that may limit the material on the bulk scale. Detailed experimental methods and results for these microscale mechanical

tests have been previously reported by Jones et al. (Ref. 9). When comparing results between the two tensile test methods, the magnitude of the UTS and the elongation at failure values for the microscale tests differ from those of the traditional tensile tests due to the reasons stated above; however, the general trend with regard to strength in the different exposure regions is consistent between the two test methods.

4.5 Density

The densities for all measured regions of HST Al-FEP and pristine material are provided in Table 5 and graphed in Figure 25. With the exceptions of R8.7 (tightly curled), R8.8 (curled), R8.11 (patched), the density of as-retrieved material did not vary significantly from pristine material (2.140 g/cm^3). Most exposure regions (besides R8.7, R8.8 and R8.11) only reached an estimated maximum temperature of 40 °C, which is too low to allow for crystallization, so no change in density was observed. A large change in density (to 2.174 g/cm^3) was observed for the curled regions, which has previously been shown to be a result of the higher on-orbit temperatures experienced in these regions (Refs. 8 and 10). At elevated temperatures chain mobility increases, allowing more polymer chains to align into the compact, crystalline state, increasing both percent crystallinity and density, as further discussed (Refs. 8 and 10).

The density of the Bay 8 Region 11 material was only marginally higher (2.146 g/cm^3) than pristine material, indicating that this region may have experienced more moderate heating. These samples were taken from directly beneath the Velcro border of the patch, which, as will be discussed, was observed to have contamination and an increase in solar absorptance. This would cause a higher temperature maximum during thermal cycling, and may account for the density increase.

Heating at 120 °C for 96 hr resulted in substantial increases in density (~0.015 g/cm^3) for most space-exposed material, but did not have a significant effect on pristine material or material from the curled regions, and the increase was much smaller (~0.004 g/cm^3) for the patched region.

The increases in density are again explained by the increase in crystallinity that occurs when polymer chains become more mobile while heated. The glass transition temperature (T_g) (α relaxation) of pristine Teflon FEP is listed from ≈83 to 150 °C in the literature, depending on hexafluoropropylene (HFP) content. Eby and Wilson report transition temperatures for FEP with densities similar to the pristine FEP examined in this report to be ≈150 and ≈127 °C for 10.7 and 17.7 mol% HFP, respectively (Ref. 11). Commercially available FEP is reported to be 20 mol% HFP (Don Farrelly, DuPont, personal communication (1999)), which would indicate that the Tg for pristine FEP would be close to 120 °C

TABLE 5.—DENSITY OF AS-RECEIVED, 120 AND 200 °C HEATED SAMPLES

HST Material Bay.Region	No. of Samples	As Retrieved		120 °C Heated		200 °C Heated	
		Density (g/cm^3)	Std. Dev.	Density (g/cm^3)	Std. Dev.	Density (g/cm^3)	Std. Dev.
Pristine Al-FEP	4	2.1397	0.0028	2.1415	0.0020	2.1597	0.0037
5.1	3	2.1361	0.0035	2.1485	0.0009	2.1840	0.0061
5.4	3	2.1438	0.0014	2.1509	0.0013	2.1823	0.0126
8.1	3	2.1378	0.0025	2.1545	0.0012	2.1970	0.0095
8.2	3	2.1403	0.0026	2.1558	0.0024	2.1901	0.0058
8.3	2	2.1408	0.0013	2.1539	0.0016	2.1863	0.0008
8.7	3	2.1714	0.0080	2.1718	0.0078	2.1879	0.0058
8.8	2	2.1744	0.0061	2.1729	0.0062	2.1852	0.0011
8.11	3	2.1458	0.0005	2.1500	0.0004	2.1809	0.0047
8.13	3	2.1385	0.0024	2.1523	0.0010	2.1875	0.0031

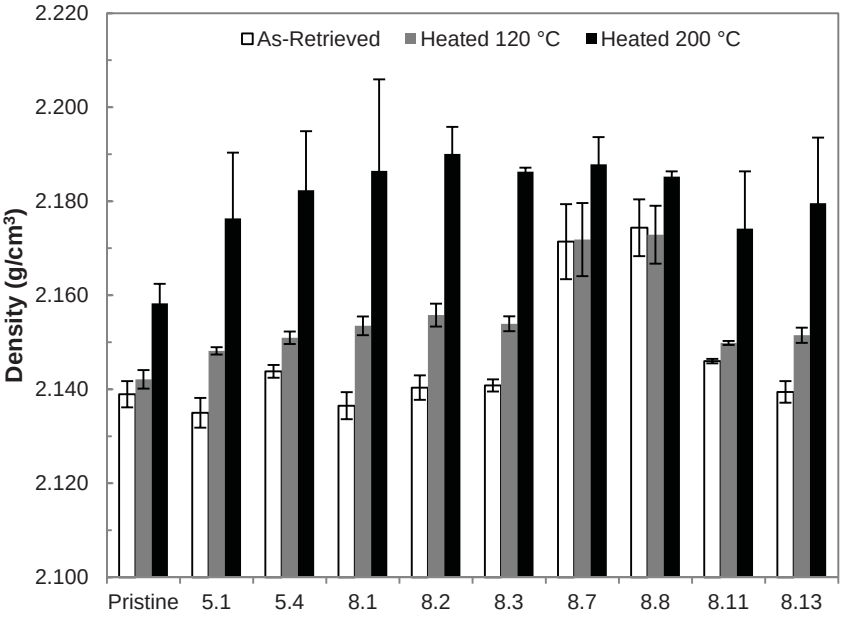

Figure 25.—Density of as-received, 120 and 200 °C heated samples. Error bars indicate the standard deviation.

based on the Eby study. In a study by de Groh and Martin, the change-of-slope temperature for density versus vacuum heat treatment temperature for pristine FEP was found to be ~126 °C (Ref. 12). Therefore, heating to 120 °C is likely to be insufficient to induce a change in crystallinity of non-irradiated FEP, as indicated in the de Groh and Martin study (Ref. 12).The density increase for HST material on heating at 120 °C indicates that solar radiation induced bond scission, increasing the mobility of polymer chains. The curled regions were already heated above 120 °C on orbit, so further heating at this temperature did not have an effect on the density of these regions. The slight density increase observed for Bay 8 Region 11 indicates that although it experienced an increase in maximum temperature, this region did not reach 120 °C on orbit.

Heating at 200 °C for 96 hr resulted in a substantial increase in density for both pristine Al-FEP and all regions of space-exposed material as compared to both pristine and 120 °C heated material. It should be noted that de Groh et al. found the on-set of melt of pristine 5 mil Al-FEP to be 244.6±3.0 °C based on DSC studies (Ref. 10), and the melt temperature was 268 °C, which is consistent with values reported in the literature. The density of 200 °C heated pristine material (2.158 g/cm^3) was significantly less than the heated material from the HST (2.174 to 2.190 g/cm^3), again indicating that space irradiation-induced scission of bonds increased mobility and crystallization on heating as compared to non-irradiated FEP. Of the HST material, the largest density increase occurred for the Bay 8 nominal material, and the smallest increases occurred for the Bay 5 nominal material, demonstrating that increased solar exposure leads to increased scission. Because there was a significant increase in density for the curled regions, it can be inferred that they did not reach 200 °C on orbit.

In the 2001 de Groh et al. study, x-ray diffraction (XRD) data was taken on pristine and retrieved HST FEP from the first three servicing missions for as-retrieved material and after heating at 200 °C. The as-retrieved space exposed FEP was found to be only very slightly higher in crystallinity (28 to 32 percent) than pristine FEP (28 percent), consistent with density data. With the exception being the servicing mission 2 (SM2) material, which has curled up tightly and was heated to 200 °C on-orbit. This material displayed both a higher density and XRD crystallinity (46 to 47 percent). The study also showed that the crystallinity of 200 °C heated samples increases, with greater increases occurring for the space exposed FEP after 200 °C. These results are consistent with the density data in this study, and provide further evidence for space irradiation-induced scission of bonds leading to increased mobility and crystallization on heating as compared to non-irradiated FEP.

4.6 Optical and Thermal Properties

The as-retrieved and 120 °C-heated solar absorptance values obtained at GSFC and GRC are provided in Table 6 and graphed in Figure 26. It should be noted that the pristine Al-FEP absorptance obtained at GRC (0.15) was slightly higher than the value obtained at GSFC (0.13). This is attributed to calibration differences between the two instruments; hence comparisons should only be made between data taken on the same instrument. As-retrieved samples from both GSFC and GRC experienced an increase in solar absorptance compared to pristine Al-FEP, with the exception of Bay 8 Region 3 (delaminated region), which was measured at GSFC without an inner layer. The GSFC absorptance of Bay 5 was slightly higher (0.16) than pristine Al-FEP (0.13), while Bay 8 had a wide range of absorptance values, with the greatest absorptance for Bay 8 Region 13 (0.27). This is the region that was patched between SM2 and SM3B, and then exposed again to space. The data trends for absorptance changes are consistent for both GSFC and GRC, with the Bay 8 hazy-white region (Region 2) and the patched regions (Regions 11 and 13) having the greatest increases in solar absorptance.

As stated previously, the GRC samples were measured with a piece of the inner layer embossed Al/Kapton/Al to best replicate the optical properties in space. As might be expected, the reflectance of the inner layer was found to have the biggest impact on the solar absorptance of the delaminated Region (R8.3), increasing the absorptance significantly as compared to the GSFC data without the inner layer.

Heating was found to increase the solar absorptance of the pristine Al-FEP by 0.09. The Bay 8 Al-FEP experienced similar increases due to heating (0.09-0.11), with the regions that were covered by patches increasing even more (0.12-0.14). Although the Bay 5 thermal cycled to a lower maximum temperature on-orbit (0 °C) than Bay 8 (40 °C), the Bay 5 Al-FEP experienced very small increases in absorptance with heating as well. The reason for this is currently unknown.

The as-retrieved and heated thermal emittance values obtained at GSFC and GRC are provided in Table 7 and graphed in Figure 27. The GSFC thermal emittance values were found to decrease for all samples except Bay 5 Region 1 and Bay 8 Region 11 (the region patched between SM2 and SM4). Emittance loss is typically associated with thickness loss of FEP, but for Bay 8 Regions 7 and 8 (the curled regions), samples may have experienced additional emittance change due to excessive heating on-orbit. Similar to the GSFC emittance values, the GRC emittance was found to decrease for all samples except Bay 5 Region 1 (also Bay 5 Region 4) and Bay 8 Region 11, the region patched between SM2 and SM4. Heating had little impact on the emittance values of the retrieved HST MLI.

TABLE 6.—SOLAR ABSORPTANCE VALUES FOR HST AND PRISTINE Al-FEP

HST Material Bay.Region	GSFC (Without Inner Layer)			GRC (With Inner Layer)				
	No. of Samples	As-Retrieved	Std. Dev.	No. of Samples	As-Retrieved	Std. Dev.	Heated	Std. Dev.
Pristine	3	0.13	-	1	0.154	0.000	0.246	0.016
5.1	3	0.16	-	2	0.217	0.021	0.225	0.040
5.4	-	-	-	2	0.253	0.043	0.299	0.063
8.1	3	0.18	0.02	2	0.189	0.038	0.301	0.035
8.2	3	0.22	0.02	1	0.249	-	0.337	-
8.3	1	0.13	-	1	0.214	-	0.326	-
8.7	3	0.19	0.01	-	-	-	-	-
8.8	3	0.23	0.01	-	-	-	-	-
8.11	3	0.26	0.05	1	0.240	-	0.359	-
8.13	3	0.27	0.01	1	0.213	-	0.349	-
8.15	-	-	-	1	0.141	-	0.301	-

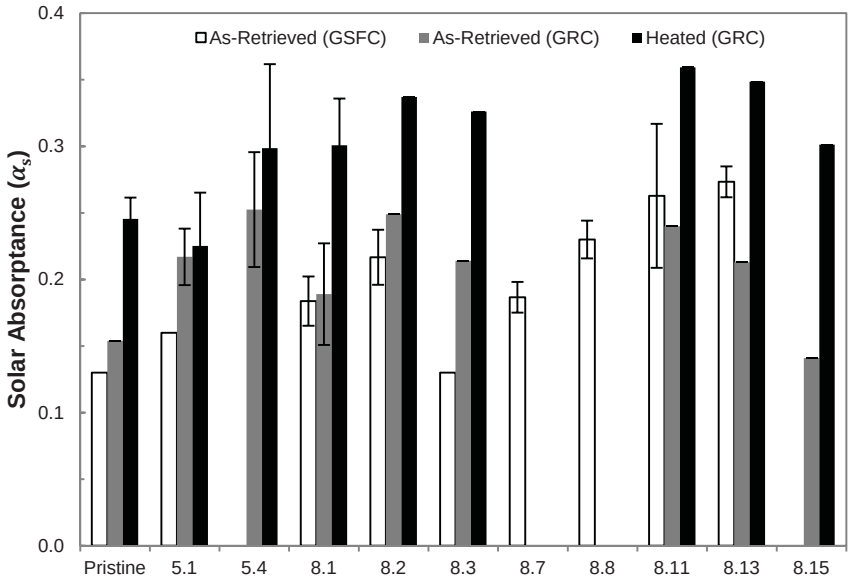

Figure 26.—As-retrieved and 120 °C heated solar absortpance values.

TABLE 7.—THERMAL EMITTANCE VALUES FOR HST AND PRISTINE Al-FEP

HST Material Bay.Region	GSFC		GRC				
	As-Retrieved	Std. Dev.	As-Retrieved	Std. Dev.	Heated	Std. Dev.	Change from heating
Pristine	0.79	0.01	0.879		0.890		0.011
5.1	0.80	0.01	0.877	0.008	0.895	0.001	0.018
5.4			0.875	0.021	0.886	0.018	0.011
8.1	0.75	0.01	0.831	0.006	0.836	0.009	0.004
8.2	0.76	0.01	0.841	-	0.861	-	0.020
8.3	0.74		0.800	-	0.805	-	0.005
8.7	0.75	0.02	-	-	-	-	-
8.8	0.73	0.01	-	-	-	-	-
8.11	0.79	0.01	0.868	-	0.874	-	0.006
8.13	0.77	-	0.830	-	0.851	-	0.021
8.15	-	-	0.030	-	0.065	-	0.035

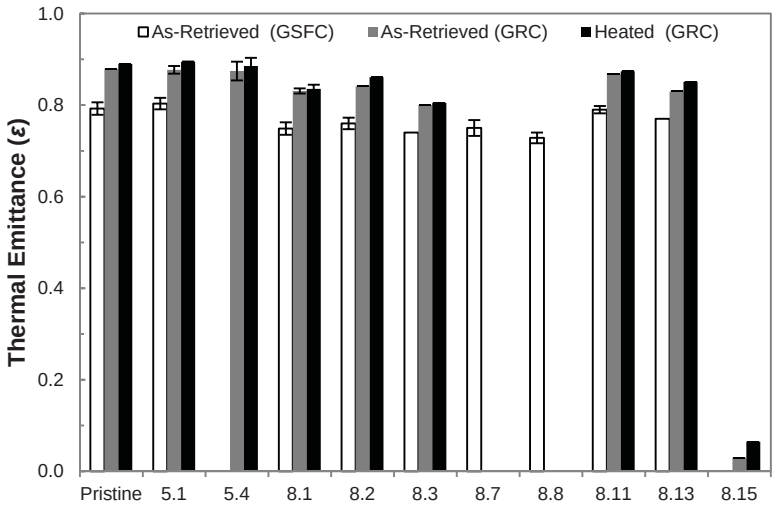

Figure 27.—As-retrieved and heated emittance values.

TABLE 8.—XPS RESULTS FOR ATOMIC PERCENT COMPOSITION

HST SM4 Material Bay.Region	Atomic %					F/C Ratio
	C	N	O	F	Si	
Pristine	33.27	0.00	0.00	66.73	0.00	2.01
5.1	19.44	1.12	36.36	22.56	20.52	1.16
8.1	39.19	2.31	6.35	50.87	1.29	1.30
8.2	39.50	2.12	5.43	52.55	0.41	1.33
8.11	59.41	4.10	18.70	15.14	2.65	0.25

4.7 X-Ray Photoelectron Spectroscopy (XPS)

The XPS analyses for pristine Al-FEP and Regions 5.1, 8.1, 8.2, and 8.11 are provided in Table 8. As expected, the pristine Al-FEP is comprised of C (33.4 percent) and F (66.7 percent). The Bay 8 nominal regions (1 and 2) were similar with an increase in C (≈39 percent), a decrease in F (≈51 percent) and the presence of O (≈6 percent), N (≈2 percent) and Si (0.4 to 1.2 percent). Bay 8 Region 11, which was patched from SM2-SM4 had a high concentration of C, possibly due to contamination from the Velcro used to attach the patch. Surprisingly, Bay 5 was found to have a significant amount of silicone contamination with the presence of 20 percent Si and 36 percent O. The back of the solar arrays are coated with DC 93-500 silicone and because Bay 5 faces towards the +V2 solar array direction, the DC 93-500 is most likely the source of contamination. As only one area of Bay 5 was tested, additional tests could determine if silicone contamination is wide spread or localized on the blanket. It would be useful to determine if this is the case, as silicone contamination could impact Ey values along with optical and thermal results.

In a 2008 study by de Groh et al., samples sectioned from Al-FEP circular thermal shields covering the bi-stem booms on the second set of HST solar arrays (retrieved after 8.25 years of space exposure) were examined with scanning electron microscopy for surface morphology and with energy dispersive spectroscopy (EDS) for surface chemistry. Pristine Al-FEP and solar-facing and anti-solar-facing thermal shield surfaces did not have any evidence of contamination, with only C and F peaks observed. However, a crazed surface texture was observed on one of the solar-grazing samples. The EDS data indicated the crazed texture is due to silicone contamination. Hence, the Bay 5 silicone contamination is consistent with contamination found on the solar-grazing surface of the retrieved solar array thermal shields, which is probably caused by contamination from the DC 93-500 silicone coating on the anti-solar side of the solar arrays.

4.8 Atomic Oxygen Erosion Yield (Ey)

Atomic oxygen Ey values determined through mass or thickness loss for the probable AO fluences are provided in Table 9. Erosion yield values were determined for Bay 8 Regions 7, 8, 11, and 13 based on the fluence only during time periods when these regions were exposed. Table 9 also provides the average Al-FEP thickness and the ratio of thickness loss (TL) Ey to mass loss (ML) Ey. The two Ey methods gave generally consistent results with each other.

The ML based Ey value of the HST SM4 Bay 8 nominal shiny FEP (Ey = 1.17×10^{-23} cm^3/atom) was found to be an order of magnitude greater than for the Bay 5 nominal shiny FEP (Ey = 1.27×10^{-24} cm^3/atom). This is attributed to the significantly higher dose of solar radiation, combined with the higher on-orbit temperature, for the solar facing blanket. It should be noted that silicone contamination on Bay 5 may have contributed somewhat to the decreased the rate of erosion. But, it is not expected that the silicone contamination would contribute an order of magnitude difference in Ey. A thick, protective layer of silicone typically is seen as a crazed surface layer, which was not at all evident in the SEM images of Bay 5 MLI (Ref. 13).

TABLE 9.—ATOMIC OXYGEN EROSION YIELD COMPARISON

HST Material Bay.Region	AO Fluence $\times 10^{-20}$ (atom/cm^2)	Avg. Mass* (g)	Mass Loss Ey (cm^3/atom)	Avg. Thickness (cm)	Thickness Loss+ Ey (cm^3/atom)	Ratio of Ey (TL)/ Ey (ML)
Pristine	-	36.837	-	0.01256	-	-
5.1	4.65	35.108	1.27E-24	0.01206	1.12E-24	0.88
8.1	4.28	22.158	1.17E-23	0.00759	1.16E-23	0.99
8.2	4.28	26.544	8.22E-24	0.00881	8.72E-24	1.06
8.3	4.28	22.810	1.12E-23	0.00736	1.21E-23	1.08
8.7	3.92	23.630	1.15E-23	0.00771	1.21E-23	1.05
8.8	3.92	23.419	1.17E-23	0.00768	1.21E-23	1.03
8.11	1.64	31.654	1.08E-23	0.01093	9.7E-24	0.90
8.13	2.69	25.282	1.49E-23	0.00824	1.60E-23	1.08

*1.27 cm diameter sample
+ Drop-Gauge Thickness

The Ey data provide evidence that solar exposure plays a significant role in the AO erosion of FEP. Erosion yield values were similar across all regions of Bay 8, with the exception of Region 2, which had a lower Ey (mass loss Ey = 8.22×10^{-24} cm^3/atom). No silicone contamination was found in this region and the reduction in Ey may be due to shadowing from adjacent patch material. The thickness reduction of HST materials comes almost entirely from erosion, with only at most 3 percent (for Bay 8 Region 8) of the total thickness change being caused by densification.

The Ey values of the HST SM4 FEP were found to be orders of magnitude greater than those determined from shuttle flight experiments such as the Evaluation of Oxygen Interaction with Materials III, reported from 5.0×10^{-26} cm^3/atom (Ref. 14) to 1.8×10^{-25} cm^3/atom (Ref. 15), the Long Duration Exposure Facility, determined to be 3.37×10^{-25} cm^3/atom for ram facing surfaces (Ref. 16) and various ram facing Materials International Space Station Experiment (MISSE) samples, determined to range from 1.28×10^{-25} cm^3/atom for MISSE 4 to 2.11×10^{-25} cm^3/atom for MISSE 2 (Refs. 17 and 18). Again, this is thought to be attributed to the effects caused by the significantly higher solar exposure of the HST materials.

The Ey values of Teflon FEP from various missions including MISSE 2, MISSE 4, MISSE 6, the Long Duration Exposure Facility (LDEF) and space exposed multilayer insulation retrieved from HST during the second servicing mission (SM2) are provided in Table 10, along with the Ey values for HST SM4 Bay 5 and Bay 8. Included in the table are the space exposure duration, solar exposure, AO fluence and AO exposure arrival. These Ey values were plotted in numerous ways including: Ey versus AO fluence, Ey versus time, Ey versus ESH and Ey versus ESH/AO ratio. The best fit was found for Ey versus ESH, and the corresponding graph is shown in Figure 28. It should be noted that although the best fit was found for Ey versus ESH, it is likely that temperature plays a critical role in the erosion process.

TABLE 10.—TEFLON FEP FROM VARIOUS MISSE MISSIONS, LDEF AND HST

Material	Mission	Duration (Yrs)	Solar Exposure (ESH)	AO Fluence ($atom/cm^2$)	AO Exposure	Ey (cm^3/atom)	Ref.
5 mil Ag-FEP	MISSE 4	1.04	1,400	2.15E+21	Ram	1.28E-25	19
5 mil Al-FEP	MISSE 7	1.5	2,400	4.22E+21	Ram	1.81E-25	20
5 mil FEP	MISSE 6	1.45	2,600	1.97E+21	Ram	1.69E-25	18
5 mil Al-FEP	MISSE 2	3.95	6,100	8.51E+21	Ram	2.11E-25	21
5 mil FEP	MISSE 2	3.95	6,300	8.43E+21	Ram	2.00E-25	17
5 mil Ag-FEP	LDEF	5.8	11,155	8.99E+21	Ram	3.37E-25	16
5 mil Al-FEP	HST SM2	6.8	33,640	3.20E+20	Sweeping AO	3.10E-24	5

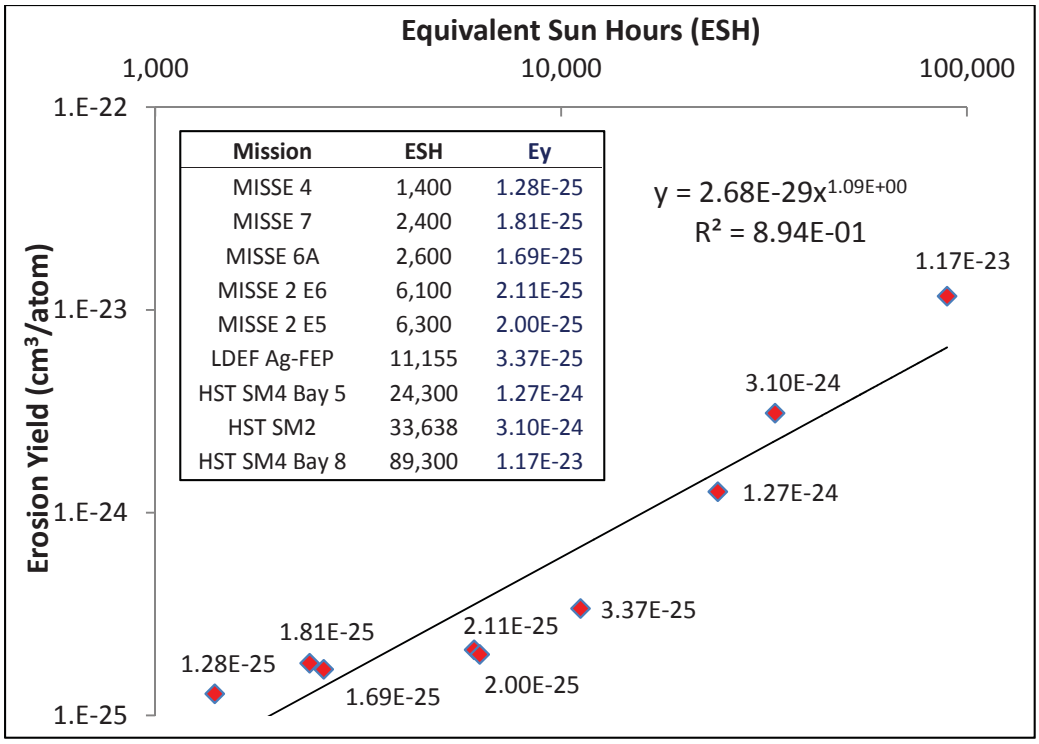

Mission	ESH	Ey
MISSE 4	1,400	1.28E-25
MISSE 7	2,400	1.81E-25
MISSE 6A	2,600	1.69E-25
MISSE 2 E6	6,100	2.11E-25
MISSE 2 E5	6,300	2.00E-25
LDEF Ag-FEP	11,155	3.37E-25
HST SM4 Bay 5	24,300	1.27E-24
HST SM2	33,638	3.10E-24
HST SM4 Bay 8	89,300	1.17E-23

Figure 28.—Erosion yield versus ESH for Teflon FEP flown from various missions.

5.0 Summary and Conclusions

Two MLI blankets retrieved from the HST during SM4 after 19.1 years in space have been analyzed for space-induced changes in thickness, density, mechanical, optical and thermal properties, and surface morphology and chemistry. In addition, atomic oxygen Ey values were determined. The blankets experienced different solar exposures and thermal cycling temperature ranges due to their positions on the telescope and each had regions with differing types of damage.

The mechanical properties of the Al-FEP outer-layers of the blankets were extremely degraded. The Bay 8 Al-FEP, which had a significantly higher solar exposure and on-orbit thermal cycling temperature, was more embrittled than the solar-grazing Bay 5 insulation, and was found to fracture like thin brittle glass. Areas on Bay 8 which had been protected by a patch for a period of time on-orbit were slightly less embrittled than areas which had been exposed for all 19.1 years. However, even the least brittle samples (Bay 5) still had only 3 percent of the elongation at failure of pristine materials. Heating pristine Al-FEP marginally decreased its strength, and had no effect on elongation. The Bay 8 MLI was too embrittled to conduct studies to assess the effect of heating, but heating Bay 5 Region 1 material reduced both the elongation and strength of the samples.

The curled and patched regions experienced increased heating on orbit, and as-retrieved material from these regions had increased density as compared to pristine material and the other regions of HST material. Heating to 120 and 200 °C resulted in larger increases in density for space-exposed material as compared to pristine material. Increases in density are correlated to increases in crystallinity. Therefore, these results indicate that irradiation in space induced polymer chain scission in the HST material, which increased the mobility of polymer chains. In turn, this increased the extent of crystallization that occurred on heating either on-orbit, or post-flight in ground studies.

All space-exposed samples experienced an increase in solar absorptance as compared to pristine Al-FEP, with the exception of Bay 8 Region 3, which is the region where the Al has delaminated from the FEP. The greatest increase in absorptance occurred in the patched areas, likely due to contamination from the patches. The thermal emittance values were found to decrease for all samples except Bay 5 Region 1 and Bay 8 Region 11 (the region patched between SM2 and SM4).

The Ey value of the HST SM4 Bay 8 nominal shiny FEP (1.37×10^{-23} cm^3/atom) was found to be an order of magnitude greater than for the Bay 5 nominal shiny FEP (1.43×10^{-24} cm^3/atom). This is attributed to the significantly higher dose of solar radiation, combined with the higher on-orbit temperature, for the solar facing blanket. The silicone contamination on Bay 5 may have decreased the Ey somewhat, but further studies are needed to assess the extent. The Ey values of the HST SM4 FEP were found to be orders of magnitude greater than those determined from prior flight missions, such as shuttle experiments (0.5 - 1.8×10^{-25} cm^3/atom), LDEF (3.37×10^{-25} cm^3/atom) and MISSE 2 experiments (2.00×10^{-25} cm^3/atom). These results support the theory that the effects of solar exposure play a significant role in the AO erosion of FEP.

Overall, the results of these tests support the proposed model for on-orbit degradation of Al-FEP, in which radiation causes chain scission of the polymers, and heating to high temperature extremes causes the Al-FEP to become more embrittled.

References

1. Tribble A. C. 1995, *The Space Environment: Implications for Spacecraft Design* (Princeton, NJ: Princeton University Press) p 155.
2. Reed R. P., Schramm R. E. and Clark A. F., "Mechanical, Thermal and Electrical Properties of Selected Polymers," *Cryogenics* February 67-82 (1973).
3. Hansen, P. A., Townsend, J. A., Yoshikawa, Y., Castro, D. J., Triolo, J. J. and Peters, W. C., SAMPE International Symposium, 43, 570, (1998).
4. Townsend, J. A., Hansen, P. A., Dever, J. A., de Groh, K. K., Banks, B. A., Wang L. and He, C., High Perform. Polym. 11, 81-99 (1999).
5. Dever, J. A., de Groh, K. K., Banks, B. A., Townsend, J. A., Barth, J. L., Thomson, S., Gregory, T. and Savage, W., High Performance Polymers, 12, 125-139 (2000).
6. American Society for Testing and Materials ASTM D 638-95, "Standard Test Method for Tensile Properties of Plastics," 1995.
7. de Groh, K. K., Waters, D. L., Mohammed, J. S., Perry, B. A. and Banks, B. A., Protection of Materials and Structures from the Space Environment, Proceedings of the ICPMSE-10J, June 12-17, 2011, Okinawa, Japan, Eds. J. Kleiman, M. Tagawa, Y. Kimoto, Astrophysics and Space Science Proceedings 32, Springer, 2013, pp 13-26; also NASA TM-2012-217644, October 2012.
8. de Groh, K. K., Gaier, J. R., Hall, R. L., Espe, M. P., Cato, D. R., Sutter, J. K. and Scheiman, D. A., High Performance Polymers 12, 83-104 (2000).
9. Jones J. S., Sharon J. A., Mohammed J. S. and Hemker K. J., Polymer Testing, 32, 602-607 (2013).
10. de Groh, K. K., Dever, J. A., Sutter, J. K., Gaier, J. R., Gummow, J. D., Scheiman, D. A. and He, C., High Performance Polymers 13, 401-420 (2001).
11. Eby, R.K. and Wilson, F.C., "Relaxations in Copolymers of Tetrafluoroethylene and Hexafluoropropylene," J. of Applied Physics, Vol. 33, No. 10, 1962, pp. 2951–2955.
12. de Groh, K. K. and Martin, M., J. Spacecraft & Rockets, 41 (3), 366-372 (2004).
13. de Groh, K. K., Finlay, K. A. and Snyder, A., High Performance Polymers, 20, 410-428 (2008).
14. Koontz, S. L., Leger, L. J., Visentine, J. T., Hunton, D. E., Cross, J. B. and Hakes, C. L., J. Spacecraft and Rockets, 32 (3), 483-495 (1995).
15. Rutledge, S. K., Banks, B. A. and Cales, M., NASA TM 106622; also AIAA-94-2628 (1994).
16. Banks, B. A., Chapter 4 in Modern Fluoropolymers: High Performance Polymers for Diverse Applications, edited by J. Scheirs, John Wiley & Sons Ltd, 1997.

17. de Groh, K. K., Banks, B. A., McCarthy, C. E., Rucker, R. N., Roberts, L. M. and Berger, L. A., High Performance Polymers, 20, 388-409 (2008).
18. de Groh, K. K., Banks, B. B., Mitchell, G. G., Yi, G. T., Guo, A., Ashmead, C. C., Roberts, L. M., McCarthy, C. E. and Sechkar, E. A., Proceedings of the ISMSE 12, Noordwijk, The Netherlands, ESA SP-705, February 2013; also NASA TM-2013-217847.
19. Dever NSMMS 2010 Dever J., de Groh, K., Nguyen, Q-V., Waters, D., Yi, G., Mitchell, G. and Guo, A., Proceedings of the NSMMS, June 28-July 1, 2010, Scottsdale, AZ, August 2010.
20. Yi, G. T., de Groh, K. K., Banks, B. A., Haloua, A., Imka, E. C. and Mitchell, G. G., Proceedings of ISMSE 12, Noordwijk, The Netherlands, ESA SP-705, February 2013; also NASA TM-2013-217848.
21. Dever, J. A., Sechkar, E. A. and Wittberg, T. N., High Performance Polymers, 20, 371-387 (2008).